Atmos. Chem. Phys. Discuss., 12, 16701–16761, 2012
www.atmos-chem-phys-discuss.net/12/16701/2012/
doi:10.5194/acpd-12-16701-2012

Atmospheric Chemistry and Physics Discussions

Cloud-resolving chemistry simulation of a Hector thunderstorm

K. A. Cummings[1], T. L. Huntemann[1,*], K. E. Pickering[2], M. C. Barth[3], W. C. Skamarock[3], H. Höller[4], H.-D. Betz[5], A. Volz-Thomas[6], and H. Schlager[4]

[1]Department of Atmospheric and Oceanic Science, University of Maryland, College Park, MD, USA
[2]Atmospheric Chemistry and Dynamics Laboratory, NASA Goddard Space Flight Center, Greenbelt, MD, USA
[3]NCAR Earth System Laboratory, National Center for Atmospheric Research, Boulder, CO, USA
[4]Deutsches Zentrum für Luft- und Raumfahrt, Oberpfaffenhofen, Germany
[5]Department of Physics, University of Munich, Munich, Germany
[6]Institut für Chemie- und Klimaforschung, Forschungszentrum Jülich, Jülich, Germany
[*]now at: National Weather Service, Silver Spring, MD, USA

Received: 30 April 2012 – Accepted: 24 May 2012 – Published: 6 July 2012

Correspondence to: K. A. Cummings (kristin@atmos.umd.edu)

Published by Copernicus Publications on behalf of the European Geosciences Union.

Abstract

Cloud chemistry simulations are performed for a Hector storm observed on 16 November 2005 during the SCOUT-O3/ACTIVE campaigns based in Darwin, Australia, with the primary objective of estimating the average production of NO per lightning flash during the storm which occurred in a tropical environment. The 3-D WRF-AqChem model (Barth et al., 2007a) containing the WRF nonhydrostatic cloud-resolving model, online gas- and aqueous-phase chemistry, and a lightning-NO_x production algorithm is used for these calculations. An idealized early morning sounding of temperature, water vapor, and winds is used to initialize the model. Surface heating of the Tiwi Islands is simulated in the model to induce convection. Aircraft observations from air undisturbed by the storm are used to construct composite initial condition chemical profiles. The idealized model storm has many characteristics similar to the observed storm. Convective transport in the idealized simulated storm is evaluated using tracer species, such as CO and O_3. The convective transport of CO from the boundary layer to the anvil region was well represented in the model, with a small overestimate of the increase of CO at anvil altitudes. Lightning flashes observed by the LIghtning detection NETwork (LINET) are input to the model and a lightning placement scheme is used to inject the resulting NO into the simulated cloud. We find that a lightning NO production scenario of 500 moles per flash for both CG and IC flashes yields anvil NO_x mixing ratios that match aircraft observations well for this storm. These values of NO production nearly match the mean values for CG and IC flashes obtained from similar modeling analyses conducted for several midlatitude and subtropical convective events and are larger than most other estimates for tropical thunderstorms. Approximately 85 % of the lightning NO_x mass was located at altitudes greater than 7 km in the later stages of the storm, which is an amount greater than found for subtropical and midlatitude storms. Upper tropospheric NO_2 partial columns computed from the model output are also considerably greater than observed by satellite for most tropical marine convective events,

ACPD
12, 16701–16761, 2012

as tropical island convection, such as Hector, is more vigorous and more productive of lightning NO_x.

1 Introduction

Nitrogen oxides (NO_x = NO + NO_2) are important trace gases in the troposphere due to their impact on photochemical ozone (O_3) formation. NO_x also influences the HO_x radicals (HO_x = HO + HO_2) which are the main oxidant of numerous chemical species. Fossil fuel combustion, biomass burning, microbial activity in soils, and lightning are considered the four major sources of tropospheric NO_x. Lightning generates less NO_x than anthropogenic sources, but does so mainly in the middle and upper troposphere where NO_x is longer-lived and more efficient at producing ozone than in the boundary layer where much of the anthropogenic NO_x is emitted. The best estimate of the global lightning-generated NO_x (LNO_x) nitrogen mass source is $5\pm3\,\mathrm{Tg\,N\,yr^{-1}}$ (Schumann and Huntrieser, 2007). The uncertainty in the source strength is due to both an uncertainty in the total number of flashes globally and the amount of NO_x per flash or per meter of flash length. The issue is further complicated by the fact that cloud-to-ground (CG) flashes and intracloud (IC) flashes may produce different amounts of NO_x. Schumann and Huntrieser (2007) provide a detailed review of three decades of research on the global LNO_x source rate.

One of the methods used in estimating the NO_x production per flash is through application of cloud-resolving models. Most of these simulations have been conducted for midlatitude and subtropical convective systems. Efforts are now being focused on tropical events using data from several atmospheric chemistry field programs recently conducted in tropical convective environments. Thunderstorms located poleward of 40° latitude in both hemispheres are noted as midlatitude systems. Those occurring between 23.5° and 40° latitude in both hemispheres and between 23.5° S and 23.5° N latitude are classified as subtropical and tropical, respectively. We focus here on simulation of a Hector thunderstorm observed during the Stratospheric-Climate Links with

ACPD
12, 16701–16761, 2012

Emphasis on the Upper Troposphere and Lower Stratosphere (SCOUT-O3; Brunner et al., 2009) and Aerosol and Chemical Transport in Tropical Convection (ACTIVE; Vaughn et al., 2008) field experiments based in Darwin, Australia. Hector is the name given to the very deep convective storms which develop over the Tiwi Islands offshore from Darwin, particularly during the transition season (November–December) prior to the monsoon onset.

Deep convection has important effects on atmospheric chemistry. It redistributes chemical constituents by rapidly moving them from the boundary layer to the upper troposphere (Chatfield and Crutzen, 1984; Dickerson et al., 1987). Here lower temperatures slow reaction rates, which generally allows chemical species in the upper troposphere to have longer lifetimes and therefore be more likely to be transported globally. Chemical consequences of the transport of boundary layer air to the upper troposphere can include changes in water vapor that lead to changes in HO_x, as well as changes in ozone (Pickering et al., 1990; 1992) and precursors. Over most of the tropics, low mixing ratios of ozone and NO_x are transported to the tropical tropopause layer (Pickering et al., 1993; Wang and Prinn, 2000; Salzmann et al., 2008) except over polluted areas, such as urban centers and biomass burning regions. Other chemical consequences include changes in aerosol concentrations and the aforementioned lightning NO production and transport. Thunderstorms inject NO_x from lightning into the middle and upper troposphere. Over relatively unpolluted regions of the tropics, LNO_x can be the dominant chemical effect of deep convection. Along with enhanced HO_x in the upper troposphere due to convectively transported water vapor and other precursors, the LNO_x leads to efficient ozone production in this layer of up to several ppbv per day (DeCaria et al., 2005). Ozone, the third most important greenhouse gas, is most effective in this role in the upper troposphere and lower stratosphere (IPCC, 2007). Therefore, better knowledge of lightning NO_x production is important for the understanding of climate forcing. Cloud-resolving models with chemistry, after evaluation with field observations, can be used for better understanding convective transport processes and LNO_x production. Cloud-scale models are valuable because they can be used to

ACPD
12, 16701–16761, 2012

simulate the transport and distribution of NO_x and its contribution to photochemistry at scales directly comparable to airborne observations in thunderstorms (Schumann and Huntrieser, 2007).

This study provides the first analysis of a cloud-resolved LNO_x simulation of deep convection in the tropics for which detailed lightning flash data and anvil NO_x measurements are available. The primary objective is to estimate the average production of NO per lightning flash in a tropical environment, as well as provide a summary of the previous research involved with tropical thunderstorm LNO_x production and with parameterizing LNO_x production in cloud-resolved models. Section 2 of this paper reviews selected cloud-resolving model studies of LNO_x, analysis of results from airborne tropical LNO_x experiments, as well as numerical modeling studies of tropical thunderstorms over the Maritime Continent. Section 3 describes the ground-based and aircraft observations of the Hector thunderstorm that occurred on 16 November 2005 during the SCOUT-O3/ACTIVE field campaign. Section 4 provides a description of the Weather Research and Forecasting Aqueous Chemistry (WRF-AqChem) model and the data used for initialization. Section 5 discusses how well the observed meteorology and chemistry is simulated over the lifetime of the thunderstorm, and Sect. 6 presents the conclusions from our cloud-resolved tropical thunderstorm simulation.

2 Background

2.1 Lightning-produced NO_x in cloud-resolving models

To simulate LNO_x production, the flash rate, the type of flash, the location of the NO source, and the amount of NO produced must be represented. Flash rates can be either predicted from storm parameters, such as cloud top height, maximum vertical velocity, ice mass fluxes, and updraft volume (Price and Rind, 1992; Petersen et al., 2005; Deierling and Petersen, 2008; Deierling et al., 2008; Barthe et al., 2010), or prescribed directly from lightning observations (DeCaria et al., 2005; Ott et al., 2010) to reduce

ACPD
12, 16701–16761, 2012

uncertainty. Likewise, the flash type can be predicted (Price and Rind, 1993; Pickering et al., 1998; Fehr et al., 2004) or prescribed from observations (DeCaria et al., 2005; Ott et al., 2007, 2010). The location of the NO source is generally near the storm core, however, the source location can reach several tens of kilometers away from the core (Höller et al., 2000; Kuhlman et al., 2009). In the volumetric approach to parameterizing LNO_x, the DeCaria et al. (2000, 2005) scheme uses the 20 dBZ reflectivity contour as the threshold for the horizontal within-cloud placement of LNO_x. The LNO_x is placed within this region in bulk, not along specific lightning flash channels. Ott et al. (2007) devised a different LNO_x placement scheme in which the resulting NO production tries to better mimic lightning flash channels by following a filamentary approach (Barthe and Barth, 2008; Ott et al., 2010). The filamentary approach uses a smaller source location, which allows NO production to represent production per flash or per meter flash length. The production of NO per flash can be derived from model results through comparisons with aircraft measurements taken within the storm anvil.

Cloud-scale simulations have been conducted using various models to estimate NO production per flash and the likely P_{IC}/P_{CG} ratio, where P_{IC} and P_{CG} are the mean NO production per IC and CG flash, respectively. Table 1 provides a list of the types of models used, as well as the LNO_x production results from each cloud-resolved simulation. For all simulated storms, the LNO_x is compared against aircraft NO_x observations in the anvils to deduce P_{IC} and P_{CG}. With the cloud-resolved two-dimensional (2-D) Goddard Cumulus Ensemble (GCE) model, Pickering et al. (1998) parameterized the LNO_x source by uniformly distributing individual flashes in the vertical within separate CG and IC lightning regions, where flash rates are predicted based on updraft vertical velocity. Seven convective events from three different regimes (midlatitude continental, tropical continental, and tropical marine) were simulated using the algorithm, and the resulting C-shaped lightning NO_x vertical profiles were developed for use in larger scale models. DeCaria et al. (2000, 2005) modified the parameterization scheme of Pickering et al. (1998) by assuming a more physically realistic non-uniform distribution of lightning channels. Gaussian distributions are used to create distinct vertical modes of flash

ACPD
12, 16701–16761, 2012

channels, and therefore also of NO_x production. Observed IC and CG flash rates are used in the model. This general technique has also been used by Ott et al. (2007, 2010) in simulating a series of midlatitude and subtropical thunderstorms. The assumptions that P_{CG} is roughly 460 moles NO per flash and P_{IC} is 75 % to 100 % of P_{CG} (DeCaria et al., 2005) provided the best comparison to the column NO_x mass computed from aircraft observations for the 12 July 1996 Stratosphere-Troposphere Experiment: Radiation, Aerosols and Ozone (STERAO-A) storm. Fehr et al. (2004) and Ott et al. (2007) both studied the production of LNO_x in the midlatitude 21 July European Lightning Nitrogen Oxides Project (EULINOX) storm using different models. Similar results for P_{CG} were obtained and both simulations showed that an IC flash produced more LNO_x than a CG flash in this storm. Ott et al. (2010) has summarized the LNO_x production results from five 3-D midlatitude and subtropical storm simulations (those of DeCaria et al., 2005; Ott et al., 2007; one additional Colorado storm and two Florida storms). Mean production per CG flash over the five storms was 500 moles flash^{-1} and the mean ratio of production per IC flash to that of a CG flash was 0.94.

Explicit electrical schemes have been used by Zhang et al. (2003b) and Barthe et al. (2007) to study LNO_x. A small, isolated, short-lived 19 July 1989 Cooperative Convective Precipitation Experiment (CCOPE) cloud with simple chemistry was simulated using the Storm Electrification Model (SEM) (Zhang et al., 2003a, b). The results indicated that the parameterization produced NO mixing ratios comparable to observations in a generic sense. A maximum NO mixing ratio of 35.8 ppbv is produced by lightning during the simulation. Barthe et al. (2007) tested an explicit electrical scheme for LNO_x using the 10 July 1996 STERAO storm. Lightning flash frequency and total path length are the key factors determined by the simulated electrical state of the storm. LNO_x dominates the NO_x budget in the upper portion of the cells with instantaneous peak mixing ratios exceeding 4 ppbv in accordance with observations. Estimated NO production is 36 moles flash^{-1}.

The cloud-scale model intercomparison performed by Barth et al. (2007b) showed that simulated NO_x variability is much larger than that seen for CO and O_3, which

ACPD
12, 16701–16761, 2012

were used as chemical tracers, demonstrating the uncertainty surrounding the placement of the NO source and its volume within the storm. Of note is that a wide range of LNO_x production rates (36-465 moles flash^{-1}) was found when six different models were used, yet they obtained similar NO_x mixing ratios in the anvil region. However, the methods of LNO_x placement varied between the models. This result, as well as the information gained from using explicit electrification schemes, indicates that there is still much to learn about LNO_x production in thunderstorms. One model used in the intercomparison was the Weather Research and Forecasting (WRF) model with a simple gas-aqueous chemistry scheme (WRF-AqChem) by Barth et al. (2007a). This model uses observed flash rates as input for the LNO_x parameterization, similar to DeCaria et al. (2005), and the results indicate that it is unlikely that lightning affects concentrations of HO_x precursors near active convection.

Based on the simulations run by Ott et al. (2010), application of their LNO_x production rates with the global annual average flash rate of 44 flashes per second yields an annual global LNO_x production of about 9 Tg N yr^{-1}, which is significantly larger than the 5 Tg N yr^{-1} estimated by Schumann and Huntrieser (2007). These results raise the question as to whether lightning flashes in tropical thunderstorms may produce less NO_x on average than flashes in midlatitude or subtropical storms. In this paper, we test whether a scenario of NO production of 500 moles per flash for both IC and CG flashes produces model-simulated NO_x mixing ratios similar to those observed in a Hector thunderstorm.

2.2 LNO_x production in tropical thunderstorms

Huntrieser et al. (2008) hypothesized that on average a tropical flash may produce less NO than a flash in a midlatitude or subtropical storm because weaker vertical wind shear in the tropics leads to shorter flash channel lengths. If the amount of nitrogen produced by lightning is better correlated with flash channel lengths than the number of strokes, subtropical and midlatitude storms may have a significant impact on the global LNO_x even though the majority of global lightning occurs in the tropics.

ACPD
12, 16701–16761, 2012

In an attempt to further investigate regional LNO_x production rates and their impact on global LNO_x, several tropical field campaigns have occurred. The first aircraft experiment specifically designed to estimate LNO_x production in the tropics was the Biomass Burning and Lightning Experiment (BIBLE-C) based in Darwin, Australia (Koike et al., 2007). On two flights, enhanced upper tropospheric NO_x mixing ratios were attributed to lightning observed several hundred kilometers upstream near the Gulf of Carpentaria. Observed lightning data along with the assumed LNO_x vertical distribution of Pickering et al. (1998) were used in conjunction with the aircraft NO_x observations to estimate LNO_x production rates of 31–73 moles flash^{-1} for one storm and 348–813 moles flash^{-1} in a second system. Based on the Tropical Convection, Cirrus, and Nitrogen Oxides Experiment (TROCCINOX) in Brazil, the LNO_x mass production for tropical thunderstorms was estimated as ∼70 moles flash^{-1}, while a subtropical thunderstorm also analyzed during the campaign had a production rate of ∼140–210 moles flash^{-1} (Huntrieser et al., 2008). The production rate for the TROCCINOX tropical event was of similar magnitude as that found for one of the BIBLE-C storms.

Huntrieser et al. (2009) analyzed thunderstorms over Northern Australia during the SCOUT-O3/ACTIVE field experiment. Similar results were noted for the thunderstorms observed in Australia as in Brazil. On 19 November 2005, tropical continental thunderstorms were found to produce the lower LNO_x production rates (121 moles flash^{-1}) compared with subtropical continental (385 moles flash^{-1}) and Hector (292–343 moles flash^{-1}) thunderstorms. Like the thunderstorms observed during TROCCINOX, the estimated vertical wind shear over Northern Australia between the anvil outflow and steering level was greater in subtropical (∼15 m s^{-1}) versus tropical (∼6 m s^{-1}) convection. For multicell Hector thunderstorms a different process may be responsible, which leads to longer flash lengths. In this scenario, the merging of several thunderstorms may influence lightning development through the presence of multiple thunderstorm centers within one convective system. The flight discussed by Huntrieser et al. (2009) was conducted during the premonsoon season, which was noted as having enhanced upper tropospheric NO_x only within storm systems

ACPD
12, 16701–16761, 2012

(Labrador et al., 2009). Later in the ACTIVE experiment (e.g., January 2006) enhanced NO_x from lightning was found over widespread regions.

Mesoscale convective systems (MCSs) over West Africa were analyzed during the African Monsoon Multidisciplinary Analysis (AMMA) wet season field campaign (Huntrieser et al., 2011). Unlike the Brazilian (Huntrieser et al., 2008) and Australian (Huntrieser et al., 2009) thunderstorms, the AMMA MCSs show a greater influence from boundary layer versus lightning NO_x. The tropical and subtropical MCSs investigated during AMMA indicate that the LNO_x production rates (70 moles flash^{-1} and 179 moles flash^{-1}, respectively) are similar to those observed in similar airmass thunderstorms during TROCCINOX. Unlike the tropical and subtropical thunderstorms observed during TROCCINOX and SCOUT-O3/ACTIVE, the difference in vertical wind shear (defined as the difference between the anvil outflow and steering level wind vectors) between subtropical and tropical AMMA MCSs is not as large (7 m s^{-1} and 9 m s^{-1}, respectively).

Based on the results from the tropical field campaigns, thunderstorms closer to the equator generally have lower LNO_x production rates, and thunderstorms investigated over Northern Australia tend to exhibit higher production rates than the thunderstorms observed in Brazil and West Africa (Höller et al., 2009). Additional research is needed to provide estimates of LNO_x production rates for a greater variety of regions in order to help reduce the large uncertainty that still exists for estimating and modeling the global LNO_x production rate. This need is highlighted by Labrador et al. (2005) in their investigation for a "best" source magnitude and vertical placement of LNO_x, and it is pointed out that the uncertainty also lies in a lack of understanding regarding the amount of energy, and associated NO molecules, produced per lightning discharge, as well as the horizontal distribution of lightning.

The in-situ measurements made during SCOUT-O3/ACTIVE over the "Maritime Continent" (the Indonesian archipelago, north Australia, and New Guinea) are well-suited for use in association with a cloud-resolving model for the purpose of studying LNO_x. Previous modeling studies indicate the feasibility of incorporating observations into

ACPD
12, 16701–16761, 2012

numerical simulations of thunderstorms in this region. This leads to consideration of how NO production per flash in a Hector storm compares with that in higher latitude storms and with other tropical thunderstorms. This paper contains the first cloud-resolved LNO_x simulation performed in the deep tropics for a storm with detailed lightning and anvil NO_x observations.

2.3 Numerical simulations of Hector thunderstorms

The "Maritime Continent" is one of the primary regions of global latent heat release that contributes to the forcing of the planetary-scale Hadley and Walker circulations. Global climate variations are directly influenced by variations in latent heat release and radiative heating within this region. These islands are excellent laboratories for the study of geographically fixed tropical convection due to their diurnal cycle of latent heat release. During the transition season of November–December, characteristic diurnal convection can be detected on 65–90 % of days over the Tiwi Islands north of Darwin, Australia (Saito et al., 2001). The Tiwis are a pair of relatively flat islands, with Melville in the east and Bathurst in the west (Fig. 1). Together they cover approximately 150 km in the east-west direction and 50 km in the north-south direction (Crook, 2001). The storms, locally known as Hector, are easily visible from Darwin, which is located 100 km to the south of the islands. Hector can reach a height of 20 km (Crook, 2001).

The Island Thunderstorm Experiment (ITEX) was conducted over the Tiwi Islands during 1988 to facilitate improved understanding of tropical island convection. Golding (1993) numerically simulated Hector using the UK Met Office mesoscale model and information from ITEX. Simulations demonstrated an island-scale confluence of sea breezes, downward transport of easterly momentum, and cold pool interactions among breeze-forced storms. While the simulations showed some agreement with observations, simulations place convergence near the center of the island whereas observations place it near the south coast. It was found that the storm development had little sensitivity to changes in cloud microphysics.

ACPD
12, 16701–16761, 2012

The Maritime Continent Thunderstorm Experiment (MCTEX) was conducted in November and December 1995 to further study deep island-based convection. Observations from MCTEX were used by Carbone et al. (2000) to develop a conceptual model of Hector development. Carbone et al. (2000) suggested that a flat, elliptical island of order 100-km resolution can act as an heat source and create an optimal condition both for the initiation of convection, as well as its subsequent organization and propagation. The majority of Hector thunderstorms develop upon the interaction of the sea breeze and gust fronts from earlier convection. Convection can free itself from the sea breeze maintenance mechanism and feed on the heated island boundary layer when evaporatively produced cold pools become cooler than the nearby sea breeze. Crook (2001) tested the conceptual model of convective development proposed by Carbone et al. (2000). The simulation suggests that the convective strength of the system increased as wind speed decreased and as wind direction turned toward the major axis of the island. Large-scale convergence and sea breezes that generate convection are driven by the heat flux. Thus, the convective strength, which was found to increase with increasing heat and moisture fluxes, was more sensitive to heat flux.

The MCTEX simulations by Saito et al. (2001) found that the diurnal evolution of convective activity over the Tiwi Islands was characterized by five stages, which capture the transition from horizontally to vertically forced convection. Shallow, non-precipitating convective cells develop over the island interior, as well as within and ahead of the sea breeze fronts during the dry and condensation stages in the morning. By afternoon the convection is forced into the vertical as sea breeze fronts from opposite sides of the island move farther inland (precipitating stage), interacting near the leeward coast and causing a sudden increase in convective activity (merging stage). As daytime heating decreases, so does the convective activity (decay stage). The diurnal evolution indicated that the horizontal island circulations and the vertical stability of the atmosphere both play important roles in the strength of the island convection. The results also suggested that tropical convection can be simulated by warm-rain processes for

ACPD
12, 16701–16761, 2012

short-range prediction, but the ice phase is important for accurate representations of vertical profiles of heat, moisture and mass budget.

3 Observations

The focus of this study is a storm observed as part of the SCOUT-O3/ACTIVE (Brunner et al., 2009; Vaughan et al., 2008) field campaigns based in Darwin, Australia. On 16 November 2005, a single-cell Hector storm developed over Bathurst Island near Apsley Strait around 14:28 LT. Figure 2 shows a series of two photographs documenting the development of the Hector thunderstorm over the Tiwi Islands. This storm and its vicinity were sampled by the DLR Falcon, M55 Geophysica, Australia's Grob G520T Egrett, and the U.K. Natural Environment Research Council Dornier aircraft. Two radars were used on this day, the Darwin Berrimah Doppler radar (12.46° S, 130.93° E) and the C-Band Polarimetric (CPOL) radar based near Gunn Point (12.25° S, 131.04° E), both owned and operated by the Centre for Australian Weather and Climate Research (CAWCR). A LIghtning detection NETwork (LINET) (Betz et al., 2004, 2007, 2008; Höller et al., 2009) of six stations was established: Point Stuart (12.58° S, 131.75° E), Cape Don (11.30° S, 131.76° E), Pirlangimpi (11.40° S, 130.41° E), Darwin (12.42° S, 130.88° E), Dundee Beach (12.78° S, 130.35° E), and Mount Bundy (13.22° S, 131.13° E). Figure 1 provides the location of the radar and LINET stations. LINET detects individual strokes, which were then organized into flashes based on time of occurrence (within 1 s) and location (within 10 km). Flash data were analyzed from 13:30 LT to 19:30 LT for the Hector storm of interest, although LINET collected data over the region for the entire day. Darwin rawinsondes were also available on this day.

The Hector cell of interest first appeared on radar at 14:28 LT over Apsley Strait between Melville and Bathurst Islands. Radar imagery shows the cell moving generally westward and intensifying by 14:58 LT, reaching a peak radar reflectivity of roughly 60 dBZ by 16:00 LT. Satellite imagery indicates anvil development by 15:03 LT. By 16:38 LT, radar observations indicate that the storm had begun to weaken. The Egrett

ACPD
12, 16701–16761, 2012

aircraft, which most extensively sampled in-anvil-cloud air, began its first in-cloud pass at 16:57 LT. The anvil size over the cell lifetime averages an area of 2365 km^2 based on IR satellite images and the Droplet Measurement Technology (DMT) cloud, aerosol and precipitation spectrometer (CAPS) on board the Egrett. The anvil moved toward the south in response to the northerly upper tropospheric winds. Radar observations indicate that the cell is nearly completely dissipated by 18:28 LT. The final in-cloud Egrett pass through the anvil ended at 18:49 LT.

As the single-cell Hector developed, the Geophysica approached the cell from the north descending stepwise from 19 km to the anvil top, arriving as the anvil was already detached and moving south. As the main convective activity was advected west, the Geophysica headed back northwest to sample overshoots of the cell, but ultimately returned to probing the environment above the main anvil by slowly descending into the top of the cloud. The two transects the Geophysica made through the anvil occurred from roughly 11–17 km over the period 17:44–18:21 LT. The Falcon initially flew further to the north and sampled outflow from a large mesoscale system that had previously developed over Papua New Guinea. The Falcon then returned to the south of the Tiwi Islands where it flew east-west cross-sections below the anvil, characterizing its vertical structure by lidar. The Egrett flew northeast-southwest oriented transects above the Falcon inside the anvil from roughly 13.2–13.8 km, whereas the Dornier characterized low-level inflow by flying large circles around the active cells. A cross calibration was performed on site in Darwin to ensure that differences in calibration standards did not cause variation in measurements amongst the aircraft.

4 Numerical model

The WRF version 2.2 model was used with a simple gas and aqueous chemistry scheme (WRF-AqChem) to simulate the 16 November 2005 storm. WRF-AqChem is described in detail by Barth et al. (2007a) and the WRF meteorological model is described by Skamarock et al. (2005). This model uses nonhydrostatic compressible

ACPD
12, 16701–16761, 2012

equations. The ice microphysics scheme (Lin et al., 1983) predicts the mass mixing ratios of cloud water, rain, cloud ice, snow, and hail. The model contains basic O_3-NO_x-CO chemistry online with 16 chemical species in the gas phase and the 5 hydrometeor reservoirs. Diurnally-varying clear-sky photolysis rates as a function of altitude are derived from the Troposphere Ultraviolet and Visible (TUV) radiation code (Madronich and Flocke, 1999). Aqueous chemistry is computed for cloud water and rain. Partitioning of species between gas and liquid hydrometeors is assumed to be in Henry's Law equilibrium for most species, but diffusion-limited mass transfer partitions highly soluble or highly reactive species. Transfer of species also occurs during the transformation of gas to ice and between hydrometeor categories following the microphysics processes. Lightning NO_x production is implemented using the DeCaria et al. (2000; 2005) schemes.

For this simulation, the model is configured to a 300×150×25 km domain with 300 grid points in the east-west direction and 150 grid points in the north-south direction at 1 km resolution and 60 grid points in the vertical direction with a variable resolution beginning at 40 m at the surface and stretching to 1840 m at the top of the domain, which is 25 km. The Tiwi Islands are represented by a landmask in the model with sensible heating at the surface applied following sunrise at 40 % of solar flux (Crook, 2001). Lightning channel segments do not follow a uniform vertical distribution (MacGorman and Rust, 1998). Instead, the vertical distribution of CG and IC flashes follow single and bimodal Gaussian distributions, respectively, where the peaks indicate where the negative charge in the cloud is at a maximum (DeCaria et al., 2000). For this simulation, the lightning channels are set to maximize at −15 °C and −60 °C, which is similar to that in midlatitude thunderstorms (−15 °C and −45 °C), except the upper mode isotherm is slightly colder because of the greater tropopause height in the tropics. NO production is tested at both 450 moles and 500 moles per CG flash and per IC flash, which are approximately the mean values from the series of midlatitude and subtropical event simulations (Ott et al., 2010) described in Sect. 2.1. These values are used

ACPD
12, 16701–16761, 2012

to determine whether NO production per flash in the Hector storm is similar to that in midlatitude or subtropical thunderstorms.

The model was initialized with a horizontally-homogeneous environment using an atmospheric profile constructed from an early morning (08:30 LT) sounding from Darwin (Fig. 3) and surface observations. Modifications were made to the temperature and moisture profiles using observations from a low-level Dornier flight and the boundary layer winds were adjusted to allow convection to form over the desired location. The sounding has a CAPE value of 1360 J kg^{-1}. The initial chemical profiles for CO, O_3, NO, and NO_2 were constructed from a composite of data from the Dornier, Falcon, Geophysica, and Egrett (Fig. 4). These data were restricted to times when the aircraft were located out of cloud and were positioned primarily to the north of the developing cell. The vertical intervals of data used in the profile construction depended on the availability of data from each aircraft. For CO and O_3, a combination of Dornier and Geophysica values were used from the surface to 3.5 km range. The values for layers between 3.5 km and 5 km were interpolated from the values at 3.5 km and 5 km. Above 5 km, Geophysica observations were used, except between 10 km and 14 km where Egrett and Geophysica CO observations were averaged and smoothed. For NO and NO_2 values, Falcon averages are used below 9 km and Egrett averages were used above this altitude. The CO profile shows spikes up to 125 ppbv in the lowest 3 km of the boundary layer, which is most likely due to upwind biomass fires in northern Australia (Allen et al., 2008). For flights made during the same field campaign when premonsoon conditions existed without the influence of biomass burning, the average CO values for the lowest 3 km were roughly 85 ppbv (Allen et al., 2008). The NO and NO_2 profiles are enhanced in the upper troposphere due to upwind lightning.

The meteorological simulation was initiated at sunrise (07:15 LT). Chemistry and trace gas transport were started in the model at 4 h 30 min into the simulation (11:45 LT), which is just prior to the initial development of the main Hector cell of interest in the model. Convection intensified in the model simulation about 2 hours earlier than in the observations (see Sect. 5). Therefore, the observed LINET flashes from

ACPD
12, 16701–16761, 2012

the storm of interest, which occurred in real time between 14:48–17:48 LT (Fig. 5), were read into the model at 10-s intervals beginning at 5 h 20 min into the simulation (12:35 LT). To keep the lightning flashes within the cell of interest, lightning read into the model was restricted to a spatial mask. The mask was adjusted at 10-minute intervals based on the movement of the cell within the model domain. There were 438 CG flashes with a mean absolute peak current value of 17.3 kA and 683 IC flashes with a mean absolute peak current value of 9.6 kA. The absolute values do not distinguish between negative and positive stroke signs. Observed flash rates peaked at approximately 15:40 LT, with a secondary peak at roughly 16:20 LT, which was followed by an extensive period of low flash rates (Fig. 5). The trend of observed flash rates generally followed the model simulated maximum vertical velocities and cloud top heights. Figure 6 illustrates the progression of LINET strokes from east to west with time.

5 Results and discussion

5.1 Meteorology

The WRF-AqChem idealized simulation reproduced a number of features of the observed storm (Table 2). A single cell appears 4 hours 40 minutes into the simulation. Given the simulation begins at sunrise (07:15 LT), the simulated cell is assumed to begin at 11:55 LT. The cell is observed by radar at about 14:30 LT, indicating the modeled Hector cell started roughly 2.5 h early. The anvil is first formed at 13 km in the model at 12:55 LT (5 h 40 min simulation time) and is first seen by Geostationary Meteorological Satellite 5 (GMS-5) at 15:03 LT, indicating about a two hour offset. The modeled cell intensifies by 14:15 LT to achieve its peak radar reflectivity of ~65 dBZ. This is close to the observed peak radar reflectivity of ~60 dBZ at 16:00 LT, with a time offset of 1.75 h. By 15:35 LT in the model, the anvil detached from the storm core and is blown toward the south.

ACPD
12, 16701–16761, 2012

The modeled anvil at 13 km dissipated by 16:15 LT (9 h simulation time) though satellite observations indicate the anvil dissipated by 18:03 LT. Thus, the anvil dissipation offset is seen to be 1.75 h. The simulated cell has dissipated in the model computed radar reflectivity at 2.5 km altitude by 15:55 LT whereas radar observations show the cell dissipating by 18:28 LT, indicating an offset of 2.5 h. These time offsets between model and observations indicate that the simulation was on average 2 h earlier than observations. It may be possible that the modification of the low-level winds to get the convection in the correct location caused an earlier convergence of the winds that initiated the convection.

The model computed radar reflectivity at 2.5 km altitude (Fig. 7 bottom) is compared with the observed radar from Gunn Point (Fig. 7 top) at an equivalent time in the storm life cycle. Both the model and the observations show the Hector cell over Bathurst Island and other scattered cells to the east. Vertical cross sections of model-computed radar reflectivity along an angle 130° from the north through the core of the storm can be compared with observed vertical radar cross sections from Gunn Point (Fig. 8). In the observations, the 20 dBZ contour (cyan) extends to 16 km. In the model simulation, the 20 dBZ contour extends to roughly 16.5 km. Note that Fig. 8 shows vertical cross sections through the observed cell (top panel) and developing model storm (bottom panel) from the southeast to northwest (left to right). However, the observed 50 dBZ contour (red/magenta interface) is roughly 7 km wide and reaches 4 km in altitude, while the model simulation indicates that the 50 dBZ contour extends to an altitude of 12.5 km and ranges in width from ∼10 km near the surface to ∼18 km around 5 km altitude. Differences in the observed and simulated 50 dBZ contour in the radar reflectivity may be due to how the ice mass concentrations are calculated in the WRF-AqChem model, which uses a bulk microphysics scheme. Overestimates of reflectivity values in the middle to upper troposphere are a well-known bias common to many bulk microphysical schemes in simulations of tropical convective systems (Lang et al., 2011). Dahl et al. (2011a, b) indicate that environments where gust fronts and sea breezes collide, as over the Tiwi Islands, and high shear environments, as in the midlatitudes, can

ACPD
12, 16701–16761, 2012

lead to an enhancement in graupel area within a simulated storm. The simulated total hydrometeors indicate that the model cloud overshoots to 20 km, which is typical of a Hector storm. The horizontal extent of the storm core and precipitation region is about the same for both model results and observations (~40 km), as is the extent of the anvil beyond the precipitation region.

Comparison of the anvil size from IR satellite images and Egrett in-cloud flight passes to modeled total hydrometeors at 13 km indicates that anvil size in the simulation is comparable to that from both of these types of observations (Fig. 9). The average extent of the anvil over the lifetime of the cell was obtained from both satellite observations and the DMT CAPS onboard the Egrett aircraft between 15:03–18:03 LT and 17:01–18:30 LT, respectively, and was estimated to be roughly 2300 km^2. This estimate is slightly smaller than the model estimate of the average anvil extent at 13 km (2757 km^2, obtained by summing the area in the model with total hydrometeors $\geq$0.01 g kg^{-1}) during the simulated anvil's lifetime (12:55-16:15 LT). Overall, the simulated storm structure compared favorably with observations, except for the extent of the 50 dBZ contour.

5.2 Carbon monoxide

Figure 10 shows a time series of vertical cross sections of CO mixing ratios from times 12:55 LT (5 h 40 min simulation time) through 15:25 LT (8 h 10 min simulation time) through the simulated cell, oriented at an angle 130° from the north through the storm core. Air that initially contained the maximum CO mixing ratios exceeding 100 ppbv in the 0–4 km region was transported to over 16 km in the core updraft region and to over 14 km in the anvil, indicating strong upward motion. In fact, modeled vertical velocities reached a maximum of 30 m s^{-1} in the core of the storm. Both the core and downwind anvil regions of the storm are largely composed of air that resided in the boundary layer prior to convection, while entrainment of environmental air with lower CO mixing ratios appears to be minimal.

To compare the simulated tracer transport with mixing ratios observed during the series of five anvil penetrations made by the Egrett aircraft over the period 16:57–18:49 LT,

ACPD
12, 16701–16761, 2012

data collected by the Egrett were averaged over 11-s intervals to yield a spatial scale equivalent to the model grid cell size, then binned into layers using the average model grid point altitudes as upper and lower boundaries. Unfortunately, in-cloud observations were only available for altitudes between 13.2–13.8 km. The model grid cells used in the comparison for each layer were selected from the simulation period from 12:55 to 14:45 LT on the condition that their total hydrometeors were $\geq 0.01\,g\,kg^{-1}$, indicating in-anvil-cloud conditions. Probability density functions (PDFs) were then calculated for the Egrett observations and compared against model layers whose average mixing ratios most closely represented the mean observed Egrett values between 13.2–13.8 km. Thus, the mean and standard deviation of CO and NO_x mixing ratios were calculated for Egrett observations between 13.2–13.8 km and model-simulated values within each model layer from 11.1–17.1 km.

The mixing ratio statistics and specified initial conditions are shown in Tables 2 and 3 for lightning NO production scenarios of 450 and 500 moles per flash. The simulated CO mixing ratio statistics within the 0.71 km thick model layer centered at 13.4 km best matched those based on the Egrett observations between 13.2–13.8 km (Table 3), indicating that vertical transport was in general well simulated by the model. Figure 11 shows the calculated PDFs of observed and simulated CO. The simulated convective transport increased the CO values above the 70.1 ppbv initial condition at many grid points, but the simulated and observed PDFs have significant differences. Egrett observations indicate a strong peak between 80–85 ppbv with just over 25 % of CO observations and a secondary peak between 95–100 ppbv with 12 % of the observations. The model distribution also shows two peaks, but they are slightly offset from the observations. Roughly 18 % of the simulated CO mixing ratio values are within the primary peak between 70–75 ppbv and a broader secondary peak covers the bins from 100-110 ppbv with roughly 9–10 % of the simulated mixing ratios in each bin. The model underestimated the number of grid points in the bins between 75–90 ppbv and 95–100 ppbv, and overestimated in every other bin. The model simulation produces CO mixing ratios of less than 65 ppbv at this altitude, which were not observed. These

ACPD
12, 16701–16761, 2012

values had to be the result of downward transport in the model from higher altitudes. The model also produced a greater frequency of large values of CO above 105 ppbv than was observed. Thus, in general, the model produced more extreme values, both large and small, than were observed. However, the total percentage of model anvil values greater than 80 ppbv was 57 %, closely matching the 62 % found in the observations in the same layer. The simulated convection increased the mean value at 13.4 km to 85.8 ppbv from the initial condition of 70.1 ppbv given 500 moles NO per flash, while the 450 mole per flash scenario, which represents a 10 % perturbation, indicated a slightly larger increase (to 86.9 ppbv). The mean observed value in this layer was 84.0 ppbv, so the simulation led to small overestimates of 1.8 ppbv (2.9 ppbv) of simulated CO for 500 (450) moles NO per flash.

The mean tracer mixing ratios observed by the Geophysica over the period 17:44–18:21 LT and simulated by the model from 12:55–14:45 LT were calculated for every model layer between 11.1–17.1 km for 500 moles per flash (Table 5). The raw tracer mixing ratios measured by the Geophysica are 5-s averages. In the layers centered at 11.4–14.1 km the simulated CO mixing ratios overestimated the Geophysica observations by roughly 25–35 % and reasonably replicated the values within ±10 % from 14.9–16.6 km. The overestimation is partially due to the CO profile used to initialize the model, which was constructed using averages of the Egrett and Geophysica observations for each model layer between 10 and 14 km. The resulting mixing ratios in this portion of the profile (70–75 ppbv) were slightly higher than those observed by the Geophysica in cloud-free air (65 ppbv). Correcting for this 10–15 ppbv offset would reduce the model overestimates to 0–20 %. Cloud observations from the Geophysica indicate that the aircraft passed in and out of the anvil (i.e., flew near cloud edge), and therefore the data may not be representative of the anvil in general. The Geophysica CO observations show only minor effects (1–4 ppbv) of convective transport, but these data represent only a very small sample of the cloud air compared with that of the Egrett (see number of observations in Tables 3, 4, and 5).

ACPD
12, 16701–16761, 2012

5.3 Nitrogen oxides

5.3.1 NO_x mixing ratios

The NO_x mixing ratio comparison focuses on the model layers centered at 12.0 km and 12.7 km, where the NO_x statistics with lightning matched the Egrett observations from 13.2–13.8 km better than the model-simulated values in the layer centered at 13.4 km. This indicates that the upper mode of the vertical distribution of IC lightning channels was likely at a higher altitude than was assumed in the model, implying that an upper mode isotherm colder than −60 °C would be appropriate for this Hector storm. LINET-observed IC strokes for this storm suggest substantial IC activity in the upper part of the anvil.

For a simulation without lightning NO production, convection brings lower NO_x mixing ratios upward to anvil levels (Fig. 12). At 14:45 LT in the simulation, at the end of the aircraft sampling period, the average NO_x mixing ratio within the layers centered at 12.0 km and 12.7 km were 60 pptv and 75 pptv, respectively, compared to 140 pptv in the layer centered at 13.4 km at the start of the simulation. These are 57 % and 46 % decreases, respectively, largely due to convective transport.

The simulation with lightning tested two lightning NO production scenarios. The 500 mole per flash scenario is based on the results of Ott et al. (2010) for midlatitude and subtropical thunderstorms, while the 450 mole per flash scenario represents a 10 % perturbation. Egrett NO_x observations are based on sequential NO and NO_x sampling. For the times when just NO was measured, a photostationary state calculation was used to estimate NO_x using observed NO values, model O_3 mixing ratios, temperature from the Darwin sounding, and $j(NO_2)$ from the TUV model. As indicated by Table 4, the model underestimated the mean anvil NO_x when 450 moles NO was used, while 500 moles NO provided a closer estimate of the observations in the mean, especially for the model layer centered at 12.0 km. The statistics indicate that a lightning NO production scenario of 500 moles per flash most closely represents the Egrett observations. Given these results, the remainder of the NO_x analysis focuses on the lightning NO production

ACPD
12, 16701–16761, 2012

scenario which uses 500 moles NO per flash. Figure 13 shows that for a simulation with lightning NO production (using the DeCaria et al. (2005) scheme with parameters as specified in Section 4), NO_x mixing ratios exceeded 3 ppbv in the storm core. Figure 14 indicates that downwind of the storm core, the anvil NO_x values slightly exceed 3 ppbv for roughly a 25 km distance. The simulated mean NO_x mixing ratio of 834 pptv (811 pptv) in the layer centered on 12.0 km (12.7 km) is seen to match within 1 % (4 %) of the observed value of 845 pptv (Table 4) for the 500 (450) moles per flash scenarios. The finding of NO_x production of 500 moles per flash is consistent with that estimated for CG flashes (523 moles flash^{-1}) based on the observed mean peak current using the relationship given by Price et al. (1997). If the Price et al. (1997) relationship is assumed to also hold for IC flashes, one would obtain an estimate of 291 moles flash^{-1}. The model results clearly indicate that an NO production per IC flash larger than this value is needed to match observed anvil NO_x observations.

The PDFs in Figure 15 contain the distribution of the model NO_x centered at 12.0 km and 12.7 km compared with that for the observed NO_x, which includes the directly measured NO_x and that estimated from the photostationary state between 13.2-13.8 km. For either layer, the PDF of the model NO_x distribution did not match the shape of the observations well. Though the mean anvil-level NO_x in both model layers using 500 moles NO per flash adequately reflects the mean of the Egrett anvil-level observations, a substantial fraction of observations between 200–400 pptv and above 2400 pptv, are missing from the simulated NO_x. The Egrett observations >2400 pptv may be from relatively fresh lightning flashes encountered by the aircraft that are not captured with the DeCaria et al. (2005) scheme in the model because the NO_x is placed into the model cloud in a bulk fashion. In this scheme the NO production is injected within the 20 dBZ contour of the storm and according to prescribed Gaussian vertical distributions (i.e., not along specific channels). As a result, the model standard deviation remains smaller than observed by 43 % and the upper end of the distribution is slightly underestimated. A broad secondary peak in model-simulated NO_x observations occurs in the bins between 1000–2400 pptv, overestimating the Egrett observations measured

ACPD
12, 16701–16761, 2012

between 13.2–13.8 km. Therefore, the magnitude of the NO_x peaks seen in the aircraft data are not reflected in the model results. Future improvements to this simulation should include a LNO_x parameterization (Ott et al., 2007; Barthe and Barth, 2008) that would inject the NO_x for individual flashes along specific channels.

The simulated NO_x mixing ratios underestimate the Geophysica measurements within the layers centered at 13.4–14.9 km, and overestimate the observations at the other layers (Table 5). Likely, the strong upward and downward motions within the simulated storm bring enhanced NO_x mixing ratios from injected lightning at mid-cloud and from above the tropopause, respectively, which leads to a simulated overestimation of NO_x observations in the lowermost and uppermost layers sampled by the Geophysica. In the layers centered at 12.0 km and 16.6 km, some of the overestimate may be due to uncertainty in the initial conditions, as the Geophysica measured only 10 pptv and 94 pptv just inside the edge of the anvil during the storm in the 12.0 km and 16.6 km layers, respectively, compared with ~120 pptv and ~145 pptv values used in the initial conditions, which were obtained from mean Egrett out-of-cloud observations. The underestimation by the model between 13.4–14.1 km (~28–79 %) may be due to the Geophysica sampling a number of fresh lightning flashes whereas the model values are more representative of lightning emissions that are more dispersed, as indicated by the much smaller standard deviations in the simulation than in the observations at these altitudes.

5.3.2 NO_2 column amounts

Satellite observations of LNO_2 have been described by Boersma et al. (2005), Bierle et al. (2009, 2010), and Bucsela et al. (2010). Figures 16 and 17 show maximum values of what a satellite might observe for the Hector storm. These figures show NO_2 tropospheric column values calculated from the model over the Tiwi Islands from the tropopause to 400 mb and 600 mb, respectively, at 14:45 LT. These are pressures within a thunderstorm cloud to which NO_2 is thought to be observable from space. Here, the tropopause is estimated as 105 mb based on the idealized sounding (Fig. 3) and the

ACPD
12, 16701–16761, 2012

climatological mean pressure of the lapse-rate tropopause from radiosonde data (Seidel et al., 2001). Actual visibility of LNO_2 from satellite may differ from these values due to the particular radiative transfer characteristics of the cloud. The largest mean partial NO_2 column values ($\geq 60\times10^{14}$ molecules cm^{-2}) are located along and just south of Apsley Strait. Low-level radar reflectivity indicates that the Hector storm is on the western coast of Bathurst Island prior to 14:45 LT (Fig. 7). With northerly upper level winds (Fig. 3) and a westward motion of the storm track across the Tiwi Islands NO_2 is transported away from the storm core and along the anvil, explaining the large mean NO_2 column values located over this region of the islands. However, NASA's Ozone Monitoring Instrument (OMI) on the Aura satellite passes over at ~13:30 LT, which was too early to observe the lightning NO_x from this Hector storm. Here we discuss tropospheric column NO_2 from the simulated Hector storm with columns computed from midlatitude storm simulations (Ott et al., 2010) and with OMI observations for tropical marine thunderstorm events from NASA's Tropical Composition, Cloud and Climate Coupling (TC^4) experiment near Costa Rica and Panama (Bucsela et al., 2010). Ott et al. (2010) indicated partial NO_2 column amounts peaked over similar regions (relative to the storm core) in the simulated storm anvils during CRYSTAL-FACE (Cirrus Regional Study of Tropical Anvils and Cirrus Layers – Florida Area Cirrus Experiment), STERAO, and EULINOX. Outside and within the Hector storm cloud the mean partial NO_2 column amounts from 400 mb to the tropopause (Fig. 16) are the same order of magnitude as the storms from CRYSTAL-FACE, STERAO, and EULINOX. The mean background values from the tropopause to 400 mb (5.8×10^{14} molecules cm^{-2}) and 600 mb (7.5×10^{14} molecules cm^{-2}) outside of the Hector storm are similar to those outside the STERAO, CRYSTAL-FACE, and several of the TC^4 storms, and slightly lower than those outside the EULINOX and the other TC^4 storms for both column depths (Bucsela et al., 2010; Ott et al., 2010). The maximum partial NO_2 column amounts from the tropopause to 400 mb (~84×10^{14} molecules cm^{-2}) and 600 mb (~103×10^{14} molecules cm^{-2}), following the end of lightning flash injections into the model, indicate that the in-cloud column amounts fall within the range of peak values

ACPD
12, 16701–16761, 2012

for the subtropical and midlatitude storms analyzed by Ott et al. (2010), but are larger than those found in the TC^4 storms.

5.3.3 NO_x vertical profiles

Figure 18 provides a comparison of the vertical profiles of the average in-cloud NO_x mixing ratios with and without lightning at 13:55 LT in the simulation. Two large peaks in NO_x (~0.95–1.05 ppbv) occur around 8.5 km and 13.5 km in the simulation with lightning. While the peak at 13.5 km corresponds well with the height of the prescribed upper mode (−60° isotherm) in the vertical distribution of LNO_x, the peak at 8.5 km is roughly 1.5 km higher than the typical altitude of the prescribed lower mode (−15° isotherm). Secondary peaks are also noted near the surface and around 6 km with ~0.5ppbv and ~0.75 ppbv NO_x, respectively. Without lightning, the profile is similar to the initial NO_x chemical profile in Fig. 4 in the lower troposphere, but with decreased values compared with initial conditions in the upper troposphere due to upward transport. With lightning, the peaks in NO_x mixing ratios are most likely due to a combination of the location where lightning is injected and vertical transport within the cloud.

The cloud-resolved model analysis of Pickering et al. (1998) produced average profiles of lightning NO_x mass for midlatitude continental, tropical continental, and tropical marine regimes all showing peaks in mass near the surface and in the upper troposphere. These C-shaped vertical distributions of lightning NO_x mass were adopted by many global CTMs. Ott et al. (2010) produced an updated set of LNO_x mass profiles for midlatitude and subtropical storms using a more realistic scheme of vertical placement of the LNO_x in the cloud-resolved model. For additional comparison against tropical convection, a vertical profile of lightning NO_x mass was computed for this idealized Hector simulation by finding the difference in NO_x between a model run with and without lightning. Figure 19 shows the percentage of N mass per kilometer due to lightning NO_xfollowing the end of model convection at 15:35 LT. Roughly 20 % of the total lightning N mass is found within the layer centered at ~7.5 km. This maximum peak corresponds to the altitude of the -15° isotherm used for the lower mode of the

ACPD
12, 16701–16761, 2012

vertical distribution of the lightning NO_x source. A second peak (~9.5 %) occurs around ~13.5 km. This altitude is similar to the altitude of the −60° isotherm used for the upper mode of the vertical distribution of the lightning NO_x source, but as indicated by the statistics for the observed and simulated NO_x mixing ratios (Table 4), the location of the upper mode in the observed storm may have been at a higher altitude. Figure 19 indicates that approximately 85 % of the LNO_x simulated in the Hector storm was located above 7 km. The vertical distribution does not resemble the tropical continental profile hypothesized by Ott et al. (2010), which had a dominant peak at 11–14 km. Instead, the vertical profile of the percentage of LNO_x mass per kilometer for the 16 November 2005 Hector storm looks more like the average midlatitude continental profile from Ott et al. (2010), except shifted roughly 3 km higher in altitude. It is possible that the directional shear within this Hector storm, discussed below, played a key role in the profile shape.

Based on these results, a lightning NO production scenario of 500 moles flash^{-1} in this Hector storm is roughly equivalent to the mean of the midlatitude and subtropical events previously studied with a similar approach. The wind speed difference, on the other hand, in the 850–200 hPa layer is only 5 m s^{-1} in the Hector system compared to the 20 and 30 m s^{-1} variation in wind speed between similar pressure levels for the STERAO and EULINOX midlatitude cases. Wind direction variation in the Hector storm, however, is significant, with the direction of the wind turning from southeast to northwest with increasing height between the low- and upper-levels of the atmosphere, respectively (Fig. 3). This leads to horizontal stretching of the storm system and possibly longer flash lengths than may be typical in the tropics. Hector, and other tropical island convection driven by localized surface heating, may create more powerful storms than are typical of the tropics and not representative of tropical thunderstorms in general. This Hector storm, along with another Hector system documented by Huntrieser et al. (2009), indicate NO production per flash is thus larger than for most other tropical thunderstorm events in the literature.

ACPD
12, 16701–16761, 2012

5.4 Ozone

Model ozone between 12:55 and 14:45 LT ranges from 6.6 ppbv to 18.6 ppbv in the anvil model layer (centered at 13.4 km) sampled by the Egrett due to both upward and downward transport. Vertical cross sections of O_3 mixing ratios for simulations without and with lightning (Fig. 20) show the upward and downward movement of O_3 within the anvil at 13:35 LT, a time of peak anvil NO_x production within the model layers centered at 12.0 km and 12.7 km. The vertical cross section with lightning shows O_3 mixing ratios are ~4 ppbv lower between 6–15 km in the storm core when compared with the vertical cross section without lightning. This slight decrease in O_3 mixing ratios in the presence of lightning is likely due to the chemical reaction of the enhanced NO mixing ratios with the O_3 molecules present in the cloud. A comparison to observations cannot be performed at the 12.0 km and 12.7 km altitudes, as O_3 was not observed on the Egrett flight. Although the Geophysica did take O_3 measurements, the WRF-AqChem simulation of the Hector thunderstorm lacks non-methane hydrocarbon (NMHC) chemistry. This makes it difficult to determine whether or not the model underestimation of observed O_3 mixing ratios (not shown) between 12.7–16.6 km (15–53 %) is due to insufficient photochemical ozone production from the absence of isoprene, the small sample size of the Geophysica observations, or the fact that the observations were taken in the anvil edge region, where the effect of convective transport of small ozone mixing ratios from the lower troposphere would have been minimal.

6 Conclusions

The 3-D WRF-AqChem model produces an idealized Hector storm with many characteristics similar to those observed. Cloud top height, horizontal dimensions of the convective cell and anvil, and peak radar reflectivity are roughly within 3 %, 17 %, and 8 % of the observations, respectively. Generally, the Hector storm evolution in the model was about 2 h ahead of the observed storm. Mean anvil-level simulated CO and NO_x,

ACPD
12, 16701–16761, 2012

when a lightning NO production scenario of 500 moles NO per flash is used, compare well with Egrett observations, although the results for CO show a small overestimate in upward convective transport to anvil levels. Though the mean anvil-level NO_x in the model adequately reflects the mean of the Egrett anvil-level observations, future improvements to the LNO_x parameterization to inject the NO_x for individual flashes along specific channels would likely improve the simulated frequency distribution of NO_x in the anvil. The Geophysica NO_x observations suggest that the upper tropospheric peak in lightning channel segments may have occurred at 1–2 km higher altitude than assumed in the model. Approximately 85 % of the total LNO_x mass resided above 7 km in the later stages of the storm. Small decreases in ozone in the region of peak lightning NO production are noted, likely due to chemical loss involving titration by the fresh NO emissions.

The mean NO production per flash in midlatitude and subtropical events previously studied with a similar approach is roughly equivalent to the results presented for this Hector storm. Analyses of aircraft NO_x observations and flash data from other tropical regions (e.g., Brazil, West Africa) suggest smaller NO production per flash in the tropics than in midlatitudes (Huntrieser et al., 2008; Huntrieser et al., 2011). Aircraft observations of another Hector storm from SCOUT-O3/ACTIVE also showed larger NO_x production per flash than in other tropical events. The upper tropospheric column NO_2 computed from the Hector simulation was of similar magnitude to that computed from midlatitude and subtropical simulations (Ott et al., 2010) and greater than that observed by OMI in tropical marine events (Bucsela et al., 2010). Therefore, we conclude that Hector, and other tropical island convection, may not be representative of tropical thunderstorms in general. The wind velocity difference between the anvil outflow and steering level of the Hector storm is less than for most midlatitude storms, but the directional difference is significant in Hector, which could lead to enhanced flash length. However, additional research is required to further assess the Huntrieser et al. (2008) hypothesis that more LNO_x may be produced per stroke in storms with greater wind shear.

ACPD
12, 16701–16761, 2012

Acknowledgements. This research was supported under NASA Aura Validation Program funding provided to Kenneth Pickering. The National Center for Atmospheric Research is supported by the National Science Foundation. The ACTIVE project was supported by the UK Natural Environment Research Council, grant NE/C512688/1 and directed by Geraint Vaughan of the University of Manchester. The authors would like to thank Heidi Huntrieser from Deutsches Zentrum für Luft- und Raumfahrt, for her comments.

References

Allen, G., Vaughan, G., Bower, K. N., Williams, P. I., Crosier, J., Flynn, M., Connolly, P., Hamilton, J. F., Lee, J. D., Saxton, J. E., Watson, N. M., Gallagher, M., Coe, H., Allan, J., Choularton, T. W., and Lewis, A. C.: Aerosol and trace-gas measurements in the Darwin area during the wet season, J. Geophys. Res., 113, D06306, doi:10.1029/2007JD008706, 2008.

Barth, M. C., Kim, S.-W., Skamarock, W. C., Stuart, A. L., Pickering, K. E., and Ott, L. E.: Simulations of the redistribution of formaldehyde, formic acid, and peroxides in the 10 July 1996 Stratospheric-Tropospheric Experiment: Radiation, Aerosols, and Ozone deep convection storm, J. Geophys. Res., 112, D13310, doi:10.1029/2006JD008046, 2007a.

Barth, M. C., Kim, S.-W., Wang, C., Pickering, K. E., Ott, L. E., Stenchikov, G., Leriche, M., Cautenet, S., Pinty, J.-P., Barthe, C., Mari, C., Helsdon, J. H., Farley, R. D., Fridlind, A. M., Ackerman, A. S., Spiridonov, V., and Telenta, B.: Cloud-scale model intercomparison of chemical constituent transport in deep convection, Atmos. Chem. Phys., 7, 4709-4731, doi:10.5194/acp-7-4709-2007, 2007b.

Barthe, C., Pinty, J.-P., and Mari, C.: Lightning-produced NO_x in an explicit electrical scheme tested in a Stratosphere-Troposphere Experiment: Radiation, Aerosols, and Ozone case study, J. Geophys. Res., 112, D04302, doi:10.1029/2006JD007402, 2007.

Barthe, C., and Barth, M. C.: Evaluation of a new lightning-produced NO_x parameterization for cloud resolving models and its associated uncertainties, Atmos. Chem. Phys., 8, 4691–4710, doi:10.5194/acp-8-4691-2008, 2008.

Barthe, C., Deierling, W., and Barth, M. C.: Estimation of total lightning from various storm parameters: A cloud-resolving model study, J. Geophys. Res., 115, D24202, doi:10.1029/2010JD014405, 2010.

ACPD

12, 16701–16761, 2012

Beirle, S., Salzmann, M., Lawrence, M. G., and Wagner, T.: Sensitivity of satellite observations for freshly produced lightning NO_x, Atmos. Chem. Phys., 9, 1077–1094, doi:10.5194/acp-9-1077-2009, 2009.

Beirle, S., Huntrieser, H., and Wagner, T.: Direct satellite observations of lightning-produced NO_x, Atmos. Chem. Phys, 10, 10965–10986, doi:10.5194/acp-10-10965-2010, 2010.

Betz, H.-D., Schmidt, K., Oettinger, W. P., and Wirz, M.: Lightning detection with 3D-discrimination of intracloud and cloud-to-ground discharges, Geophys. Res. Lett., 31, L11108, doi:10.1029/2004GL019821, 2004.

Betz, H.-D., Schmidt, K., Fuchs, B., Oettinger, W. P., and Höller, H.: Cloud lightning: Detection and utilization for total lightning measured in the VLF/LF regime, J. Lightning Res., 2, 1–17, 2007.

Betz, H.-D., Schmidt, K., and Oettinger, W. P.: LINET – An International VLF/LF Lightning Detection Network in Europe, in: Lightning: Principles, Instruments and Applications, edited by: Betz, H.-D., Schumann, U., and Laroche, P., Springer, Dordrecht, The Netherlands, Chapter 5, 2008.

Boersma, K. F., Eskes, H. J., Meijer, E. W., and Kelder, H. M.: Estimates of lightning NO_x production from GOME satellite observations, Atmos. Chem. Phys., 5, 3047–3104, doi:10.5194/acpd-5-3047-2005, 2005.

Brunner, D., Siegmund, P., May, P. T., Chappel, L., Schiller, C., Miller, R., Peter, T., Fueglistaler, S., MacKenzie, A. R., Fix, A., Schlager, H., Allen, G., Fjaeraa, A. M., Streibel, M., and Harris, N. R. P.: The SCOUT-O3 Darwin Aircraft Campaign: rationale and meteorology, Atmos. Chem. Phys., 9 93–117, doi:10.5194/acp-9-93-2009, 2009.

Bucsela, E. J., Pickering, K. E., Huntemann, T. L., Cohen, R. C., Perring, A., Gleason, J. F., Blakeslee, R. J., Albrecht, R. I., Holzworth, R., Cipriani., J. P., Vargar-Navarro, D., Mora-Segura, I., Pacheco-Hernandez, A., and Laporte-Molina, S.: Lightning-generated NO_x seen by the Ozone Monitoring Instrument during NASA's Tropical Composition, Cloud and Climate Coupling Experiment (TC^4), J. Geophys. Res., 115, D00J10, doi:10.1029/2009JD013118, 2010.

Carbone, R. E., Keenan, T. D., Hacker, J., and Wilson, J. W.: Tropical island convection in the absence of significant topography. Part I: Life cycle of diurnally forced convection. Mon. Weather Rev., 128, 3459–3480, 2000.

Chatfield, R. B. and Crutzen, P. J.: Sulfur dioxide in remote ocean air: Cloud transport of reactive precursors, J. Geophys. Res., 89, 7111–7132, 1984.

ACPD

12, 16701–16761, 2012

Crook, N. A.: Understanding Hector: the dynamics of island thunderstorms, Mon. Weather Rev., 129, 1550–1563, 2001.

Dahl, J. M. L., Höller, H., and Schumann, U.: Modeling the flash rate of thunderstorms – Part I: Framework, Mon. Weather Rev., 139, 3093–3111, doi:10.1175/MWR-D-10-05031.1, 2011a.

Dahl, J. M. L., Höller, H., and Schumann, U.: Modeling the flash rate of thunderstorms. Part II: Implementation, Mon. Weather Rev., 139, 3112–3124, doi:10.1175/MWR-D-10-05032.1, 2011b.

DeCaria, A. J., Pickering, K. E., Stenchikov, G. L., Scala, J. R., Stith, J. L., Due, J. E., Ridley, B. A., and Laroce, P.: A cloud-scale model study of lightning-generated NO_x in an individual thunderstorm during STERAO-A, J. Geophys. Res., 105, 11601–11616, 2000.

DeCaria, A. J., Pickering, K. E., Stenchikov, G. L., and Ott, L. E.: Lightning-generated NO_x and its impact on tropospheric ozone production: A 3-D modeling study of a STERAO-A thunderstorm, J. Geophys. Res., 110, D14303, doi:10.1029/2004JD005556, 2005.

Deierling, W. and Petersen, W. A.: Total lightning activity as an indicator of updraft characteristics, J. Geophys. Res., 113, D16210, doi:10.1029/2007JD009598, 2008.

Deierling, W., Petersen, W. A., Latham, J., Ellis, S., and Christian, H. J.: The relationship between lightning activity and ice fluxes in thunderstorms, J. Geophys. Res., 113, D15210, doi:10.1029/2007JD009700, 2008.

Dickerson, R. R., Huffman, G. J., Luke, W. T., Nunnermacker, L. J., Pickering, K. E., Leslie, A. C. D., Lindsey, C. G., Slinn, W. G. N., Kelly, T. J., Daum, P. H., Delany, A. C., Greenberg, J. P., Zimmerman, P. R., Boatman, J. F., Ray, J. D., and Steadman, D. H.: Thunderstorms: An important mechanism in the transport of air pollutants, Science, 235, 460–465, 1987.

Fehr, T., Höller, H., and Huntrieser, H.: Model study on production and transport of lightning-produced NO_x in a EULINOX supercell storm, J. Geophys. Res., 109, D09102, doi:10.1029/2003JD003935, 2004.

Golding, B. W.: A numerical investigation of tropical island thunderstorms, Mon. Weather Rev., 121, 1417–1433, 1993.

Höller, H., Betz, H.-D., Schmidt, K., Calheiros, R. V., May, P., Houngninou, E., and Scialom, G.: Lightning characteristics observed by a VLF/LF lightning detection network (LINET) in Brazil, Australia, Africa and Germany, Atmos. Chem. Phys., 9, 7795–7824, doi:10.5194/acp-9-7795-2009, 2009.

Huntrieser, H., Schlager, H., Roiger, A., Lichtenstern, M., Schumann, U., Kurz, C., Brunner, D., Schwierz, C., Richter, A., and Stohl, A.: Lightning-produced NO_x over Brazil

ACPD

12, 16701–16761, 2012

during TROCCINOX: airborne measurements in tropical and subtropical thunderstorms and the importance of mesoscale convective systems, Atmos. Chem. Phys., 7, 2987–3012, doi:10.5194/acp-7-2987-2007, 2007.

Huntrieser, H., Schumann, U., Schlager, H., Höller, H., Giez, A., Betz, H.-D., Brunner, D., Forster, C., Pinto Jr., O., and Calheiros, R.: Lightning activity in Brazilian thunderstorms during TROCCINOX: implications for NO_x production, Atmos. Chem. Phys., 8, 921–953, doi:10.5194/acp-8-921-2008, 2008.

Huntrieser, H., Schlager, H., Lichtenstern, M., Roiger, A., Stock, P., Minikin, A., Höller, H., Schmidt, K., Betz, H.-D., Allen, G., Viciani, S., Ulanovsky, A., Ravegnani, F., and Brunner, D.: NO_x production by lightning in Hector: first airborne measurements during SCOUT-O3/ACTIVE, Atmos. Chem. Phys., 9, 8377–8412, doi:10.5194/acp-9-8377-2009, 2009.

Huntrieser, H., Schlager, H., Lichtenstern, M., Stock, P., Hamburger, T., Höller, H., Schmidt, K., Betz, H.-D., Ulanovsky, A., and Ravegnani, F.: Mesoscale convective systems observed during AMMA and their impact on the NO_x and O_3 budget over West Africa, Atmos. Chem. Phys., 11, 2503–2536, doi:10.5194/acp-11-2503-2011, 2011.

IPCC: Climate Change 2007: The Physical Science Basis. Contribution of Working Group I to the Fourth Assessment Report of the Intergovernmental Panel on Climate Change, edited by:Solomon, S., Qin, D., Manning, M., Chen, Z., Marquis, M., Averyt, K. B., Tignor, M., and Miller, H. L., Cambridge, United Kingdom and New York, NY, USA, 996 pp., 2007.

Koike, M., Kondo, Y., Kita, K., Takegawa, N., Nishi, N., Kashihara, T., Kawakami, S., Kudoh, S., Blake, D., Shirai, T., Liley, B., Ko, M., Miyazaki, Y., Kawasaki, Z., and Ogawa, T.: Measurements of reactive nitrogen produced by tropical thunderstorms during BIBLE-C, J. Geophys. Res., 112, D18304, doi:10.1029/2006JD008193, 2007.

Kuhlman, K. M., MacGorman, D. R., Biggerstaff, M. I., and Krehbiel, P. R.: Lightning initiation in the anvils of two supercell storms, Geophys. Res. Lett., 36, L07802, doi:10.1029/2008GL036650, 2009.

Labrador, L. J., von Kuhlmann, R., and Lawrence, M. G.: The effects of lightning- produced NO_x and its vertical distribution on atmospheric chemistry: sensitivity simulations with MATCH-MPIC, Atmos. Chem. Phys., 5, 1815-1834, 2005, http://www.atmos-chem-phys.net/5/1815/2005/.

Labrador, L., Vaughan, G., Heyes, W., Waddicor, D., Volz-Thomas, A., Pätz, H.-W., and Höller, H.: Lightning-produced NO_x during the Northern Australian monsoon; results from the ACTIVE campaign, Atmos. Chem. Phys., 9, 7419–7429, doi:10.5194/acp-9-7419-2009, 2009.

ACPD

12, 16701–16761, 2012

Lang, S. E., Tao, W.-K., Zeng, X., and Li, Y.: Reducing the biases in simulated radar reflectivities from a bulk microphysics scheme: Tropical convective systems, J. Atmos. Sci., 68, 2306–2320, 2011.

Leriche, M., Cautenet, S., Barth, M., and Chaumerliac, N.: Modelling of the July 10 STERAO storm with the RAMS model: Chemical species redistribution including gas phase and aqueous phase chemistry, in: Air Pollution Modeling and Its Application XVIII, edited by: Borrego, C. and Renner, E., 433–442, Elsevier, Amsterdam, The Netherlands, 2007.

Lin, Y.-L., Farley, R. D., and Orville, H. D.: Bulk parameterization of the snow field in a cloud model, J. Clim. Appl. Meteorol., 22, 1065–1092, 1983.

MacGorman, D. R. and Rust, W. D.: The Electrical Nature of Storms, 422 pp., Oxford Univ. Press, New York, USA, 1998.

Madronich, S. and Flocke, S.: The role of solar radiation in atmospheric chemistry, in Handbook of Environmental Chemistry, edited by: Boule, P., Springer, New York, USA, 1–26, 1999.

Ott, L. E., Pickering, K. E., Stenchikov, G. L., Huntrieser, H., and Schumann, U.: Effects of lightning NO_x production during the 21 July European Lightning Nitrogen Oxides Project storm studied with a three-dimensional cloud-scale chemical transport model, J. Geophys. Res., 112, D05307, doi:10.1029/2006JD007365, 2007.

Ott, L. E., Pickering, K. E., Stenchikov, G. L., Allen, D. J., DeCaria, A. J., Ridley, B., Lin, R.-F., Wang, D., Lang, S., and Tao, W.-K.: Production of lightning NO_x and its vertical distribution calculated from 3-D cloud-scale chemical transport model simulations, J. Geophys. Res., 115, D04301, doi:10.1029/2009JD011880, 2010.

Petersen, W. A., Christian, H. J., and Rutledge, S. A.: TRMM observations of the global relationship between ice water content and lightning, Geophys. Res. Lett., 32, L14819, doi:10.1029/2005GL023236, 2005.

Pickering, K. E., Thompson, A. M., Dickerson, R. R., Luke, W. T., and McNamara, D. P.: Model calculations of tropospheric ozone production potential following observed convective events, J. Geophys. Res., 95, 14049–14062, 1990.

Pickering, K. E., Thompson, A. M., Scala, J. R., Tao, W.-K., Dickerson, R. R., and Simpson, J.: Free tropospheric ozone production following entrainment of urban plumes into deep convection, J. Geophys. Res., 97, 17985–18000, 1992.

Pickering, K. E., Thompson, A. M., Tao, W., and Kucsera, T. L.: Upper tropospheric ozone production following mesoscale convection during STEP/EMEX, J. Geophys. Res., 98, 8737–8749, 1993.

ACPD
12, 16701–16761, 2012

Pickering, K. E., Wang, Y., Tao, W.-K., Price, C., and Müller, J.-F.: Vertical distribution of lightning NO_x for use in regional and global chemical transport models, J. Geophys. Res., 103, 31203–31216, 1998.

Price, C. and Rind, D.: A simple lightning parameterization for calculating global lightning distributions, J. Geophys. Res., 97, 9919–9933, doi:10.1029/92JD00719, 1992.

Price, C. and Rind, D.: What determines the cloud-to-ground lightning fraction in thunderstorms?, Geophys. Res. Lett., 20, 463-466, 1993.

Price, C., Penner, J., and Prather, M.: NO_x from lightning 1. Global distribution based on lightning physics, J. Geophys. Res., 102, 5929–5941, 1997.

Saito, K., Keenan, T., Holland, G., and Puri, K.: Numerical simulation of the diurnal evolution of tropical island convection over the Maritime Continent, Mon. Weather Rev., 129, 378–400, 2001.

Salzmann, M., Lawrence, M. G., Phillips, V. T. J., and Donner, L. J.: Cloud resolving model study of the roles of deep convection for photo-chemistry in the TOGA COARE/CEPEX region, Atmos. Chem. Phys., 8, 2741–2757, doi:10.5194/acp-8-2741-2008, 2008.

Schumann, U., and Huntrieser, H.: The global lightning-induced nitrogen oxides source, Atmos. Chem. Phys., 7, 3823–3907, doi:10.5194/acp-7-3823-2007, 2007.

Seidel, D. J., Ross, R. J., Angell, J. K., and Reid, G. C.: Climatological characteristics of the tropical tropopause as revealed by radiosondes, J. Geophys. Res., 106, 7857–7878, doi:10.1029/2000JD900837, 2001.

Skamarock, W. C., Klemp, J. B., Dudhia, J., Gill, D., Barker, D., Wang, W., and Powers, J. G.: A description of the Advanced Research WRF Version 2., Technical Note NCAR/TN-468+STR, NCAR, Boulder, Colorado, USA, 2005.

Vaughan, G., Schiller, C., MacKenzie, A. R., Bower, K., Peter, T., Schlager, H., Harris, N. R. P., and May, P. T.: SCOUT-O3/ACTIVE: High-altitude aircraft measurements around deep tropical convection, B. Am. Meteor. Soc., 89, 647–662, 2008.

Wang, C. and Prinn, R.: On the roles of deep convective clouds in tropospheric chemistry, J. Geophys. Res., 105, 22269–22298, 2000.

Zhang, X., Helsdon Jr., J. H., and Farley, R. D.: Numerical modeling of lightning-produced NO_x using an explicit lightning scheme: 1. Two-dimensional simulation as a “proof of concept”, J. Geophys. Res., 108, 4579, doi:10.1029/2002JD003224, 2003a.

ACPD

12, 16701–16761, 2012

Zhang, X., Helsdon Jr., J. H., and Farley, R. D.: Numerical modeling of lightning-produced NO_x using an explicit lightning scheme: 2. Three-dimensional simulation and expanded chemistry, J. Geophys. Res., 108, 4580, doi:10.1029/2002JD003225, 2003b.

ACPD

12, 16701–16761, 2012

Table 1. Summary of cloud-resolved simulations of LNO_x production.

Model	Moles NO per CG flash	P_{IC}/P_{CG}	Field Campaign	Region	Reference
2-D GCE	200–500	> 0.5	STERAO-A	Midlatitude	DeCaria et al. (2000, 2005)
3-D GCE/CSCTM	460	0.75–1.00			
MM5	330	1.4	EULINOX	Midlatitude	Fehr et al. (2004)
3-D GCE/CSCTM	360	1.15	EULINOX	Midlatitude	Ott et al. (2007)
3-D GCE/MM5/CSCTM	500*	0.94*	STERAO-A; EULINOX; CRYSTAL-FACE	3 midlatitude; 2 subtropical	Ott et al. (2010)
Intercomparison**	36–465	~0.1–1.0	STERAO-A	Midlatitude	Barth et al. (2007b)

* indicates that the value is a mean value based on five storm simulations; ** Intercomparison of six models simulating LNO_x; GCE: Goddard Cumulus Ensemble model; CSCTM: Cloud-Scale Chemical Transport Model; MM5: Penn State/NCAR Mesoscale Model version 5; STERAO-A: Stratosphere-Troposphere Experiment: Radiation, Aerosols and Ozone; EULINOX: European Lightning Nitrogen Oxides Project; CRYSTAL-FACE: Cirrus Regional Study of Tropical Anvils and Cirrus Layers – Florida Area Cirrus Experiment

ACPD
12, 16701–16761, 2012

Table 2. Summary of the observed and simulated features in the 16 November 2005 Hector thunderstorm.

	Observations	Simulation
Initial radar indication of cell at 2.5 km	14:28 LT	11:55 LT
Initial anvil development at 13 km	15:03 LT	12:55 LT
Peak radar reflectivity at 2.5 km	16:00 LT (~60 dBZ)	14:15 LT (~65 dBZ)
Initial anvil dissipation at 13 km	18:03 LT	16:15 LT
Complete cell dissipation at 2.5 km	18:28 LT	15:55 LT

ACPD
12, 16701–16761, 2012

Table 3. Egrett observed and simulated CO mixing ratio statistics for the layer centered at 13.4 km. Simulated values are based on a lightning NO production scenario of 450 and 500 moles flash^{-1}. The layer centered at 13.4 km contained 351 11-s Egrett observations and 1268 simulated values.

	Initial Condition CO (ppbv)	Observed Anvil CO (ppbv)	Simulated Anvil CO (ppbv)	
			450 moles NO flash^{-1}	500 moles NO flash^{-1}
Mean	70.1	84.0	86.9	85.8
Maximum	–	114.5	117.4	117.4
Standard Deviation	–	9.9	15.3	14.8

ACPD
12, 16701–16761, 2012

Table 4. Statistics for the Egrett observed NO_x mixing ratios for the layer centered at 13.4 km compared with the simulated NO_x mixing ratios for the layers centered at 12.0 km and 12.7 km. Simulated values are based on a lightning NO production scenario of 450 and 500 moles flash^{-1}. The layer centered at 12.0 km (12.7 km) contained 338 11-s Egrett observations and 2236 (1782) simulated values.

450 moles NO per Flash				
	Initial Condition NO_x(pptv)	Observed Anvil NO_x (pptv)	Simulated Anvil NO_x (pptv)	
			12.0 km	12.7 km
Mean	140	845	758	739
Maximum	–	5139	2678	2606
Standard Deviation	–	1140	692	602
500 moles NO per Flash				
	Initial Condition NO_x (pptv)	Observed Anvil NO_x (pptv)	Simulated Anvil NO_x (pptv)	
			12.0 km	12.7 km
Mean	140	845	834	811
Maximum	–	5139	2970	2889
Standard Deviation	–	1140	769	670

ACPD
12, 16701–16761, 2012

Table 5. Statistics for the Geophysica observed and simulated tracer mixing ratios for multiple layers centered at 11.4–16.6 km. Simulated values are based on a lightning NO production scenario of 500 moles flash^{-1}.

Altitude (km)	# Obs	Mean CO (ppbv)		Maximum CO (ppbv)		CO Standard Deviation (ppbv)	
		Observed	Simulated	Observed	Simulated	Observed	Simulated
11.4	1	67.6	90.5	67.6	117.0	–	10.8
12.0	11	66.1	93.8	67.4	124.5	0.6	10.4
12.7	20	68.6	91.0	71.4	123.3	1.0	11.8
13.4	33	67.9	85.8	74.5	117.4	4.0	15.3
14.1	43	65.1	80.8	68.2	118.0	1.9	18.1
14.9	42	66.0	75.3	72.2	122.9	4.7	20.7
15.7	66	70.3	65.8	75.5	126.4	4.9	19.1
16.6	32	59.3	63.0	63.9	124.6	2.7	15.2
Altitude (km)	# Obs	Mean NO_x (ppbt)		Maximum NO_x (ppbt)		NO_x Standard Deviation (ppbt)	
		Observed	Simulated	Observed	Simulated	Observed	Simulated
11.4	0	–	639	–	2840	–	700
12.0	4	10	834	13	2970	4	769
12.7	20	476	811	922	2889	258	670
13.4	16	984	705	3028	2745	967	617
14.1	30	2826	587	3363	2540	621	604
14.9	38	597	475	1654	2248	548	534
15.7	52	162	364	243	2036	31	408
16.6	32	94	432	118	1760	7	283

ACPD
12, 16701–16761, 2012

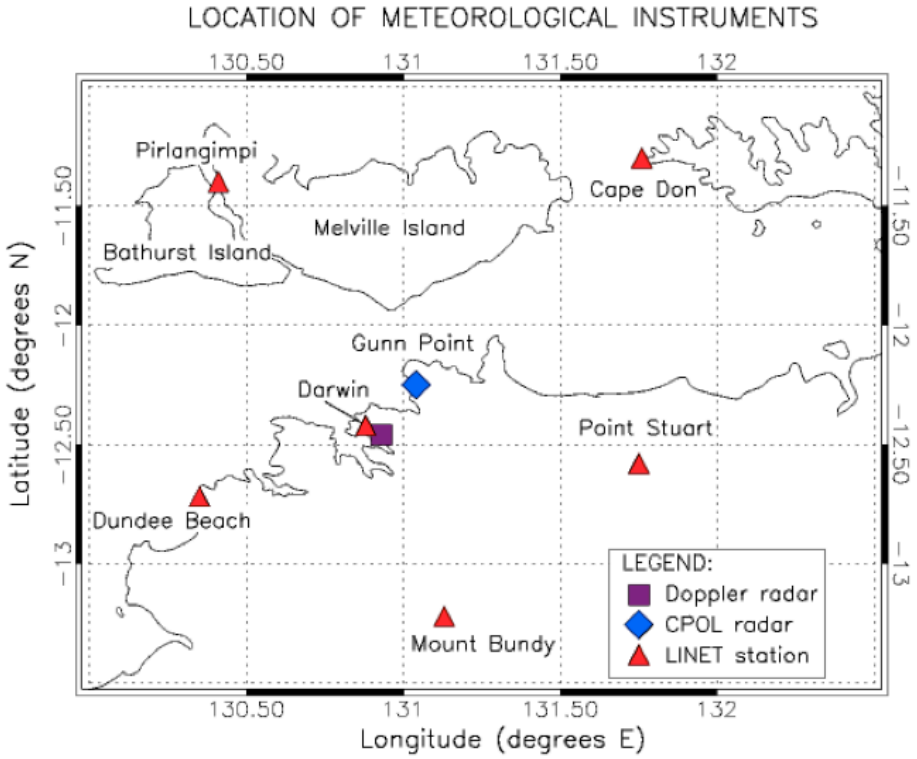

Fig. 1. Location of the two CAWCR radar and six LINET stations involved in the campaign.

ACPD
12, 16701–16761, 2012

Fig. 2. Development of the Hector thunderstorm over the Tiwi Islands on 16 November 2005 during the SCOUT-O3/ACTIVE field campaign. From left to right, the photos indicate the stage of single-cell development at ~16:19 LT and ~17:09 LT, respectively.

ACPD
12, 16701–16761, 2012

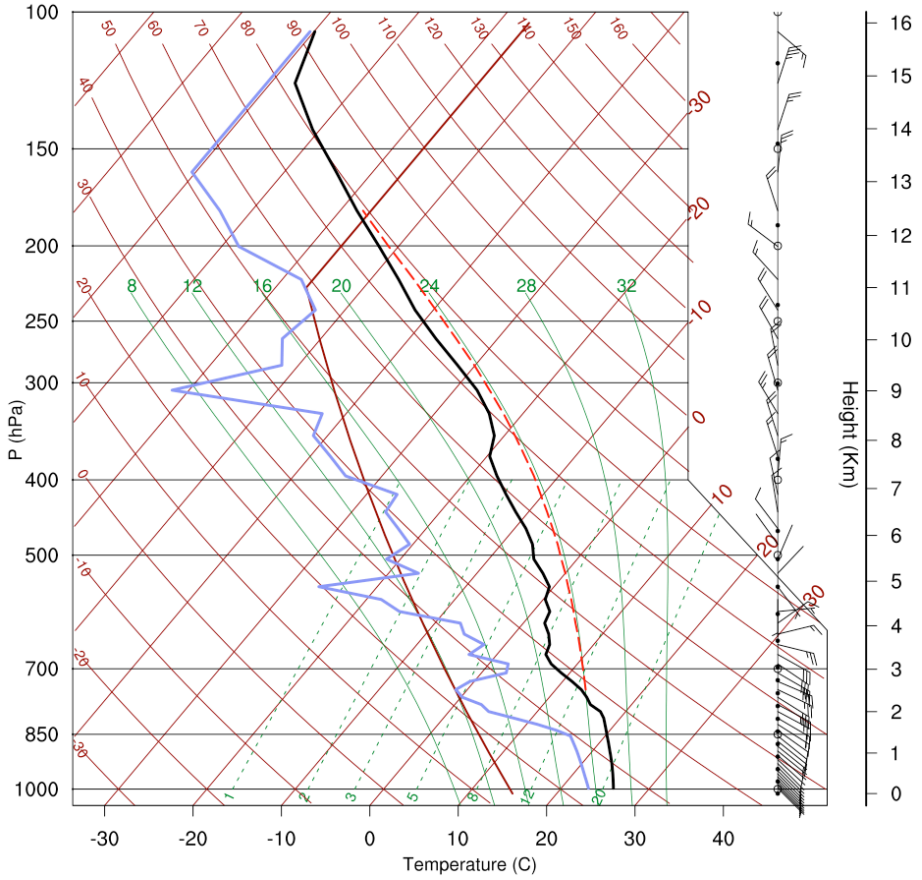

Fig. 3. Sounding used in the horizontally-homogeneous simulation initialization. Temperature and dew point are plotted as black and blue lines, respectively. Wind speed is reported in knots, where a full barb is equivalent to 10 knots.

ACPD
12, 16701–16761, 2012

Cloud-resolving chemistry simulation of a Hector thunderstorm

K. A. Cummings et al.

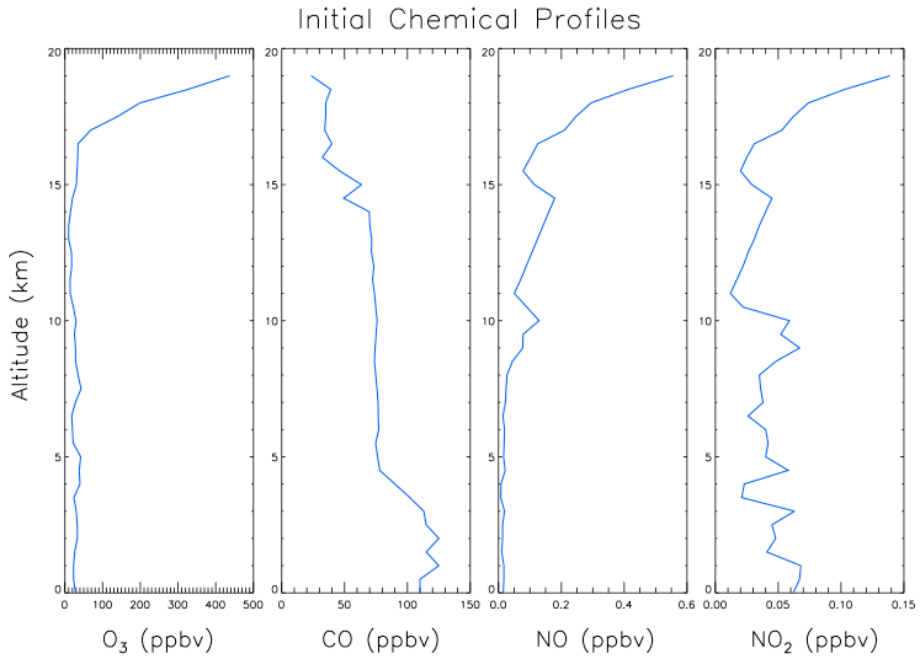

Fig. 4. Initial chemical profiles based on composite of Dornier, Falcon, Geophysica, and Egrett measurements.

ACPD
12, 16701–16761, 2012

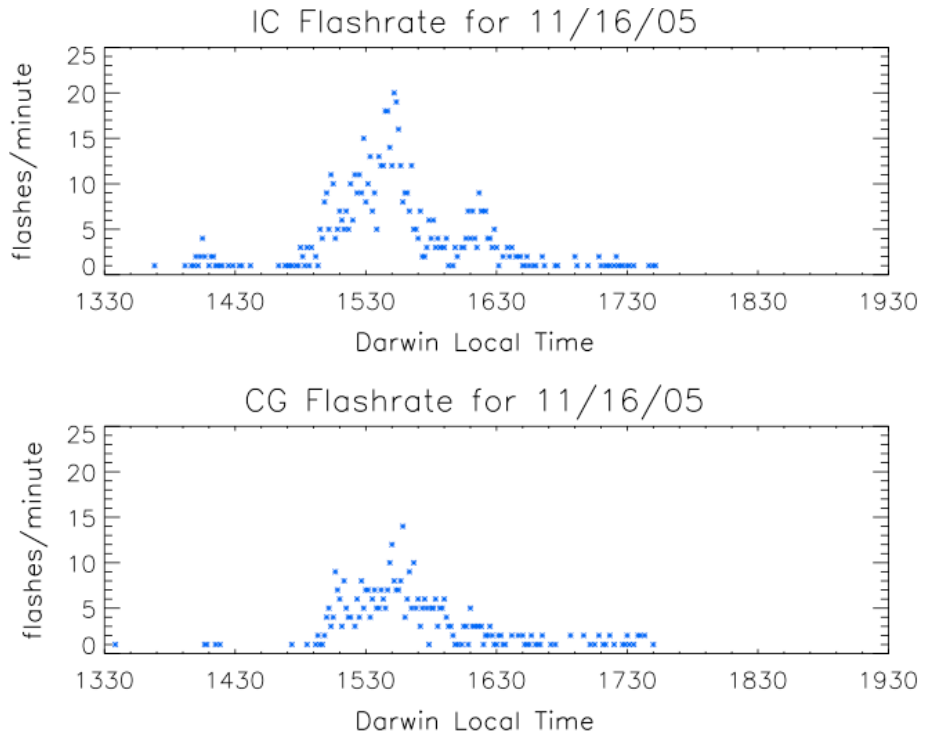

Fig. 5. Time series of IC and CG flashes per minute for 13:30–19:30 LT for the selected Hector storm.

ACPD
12, 16701–16761, 2012

Cloud-resolving chemistry simulation of a Hector thunderstorm

K. A. Cummings et al.

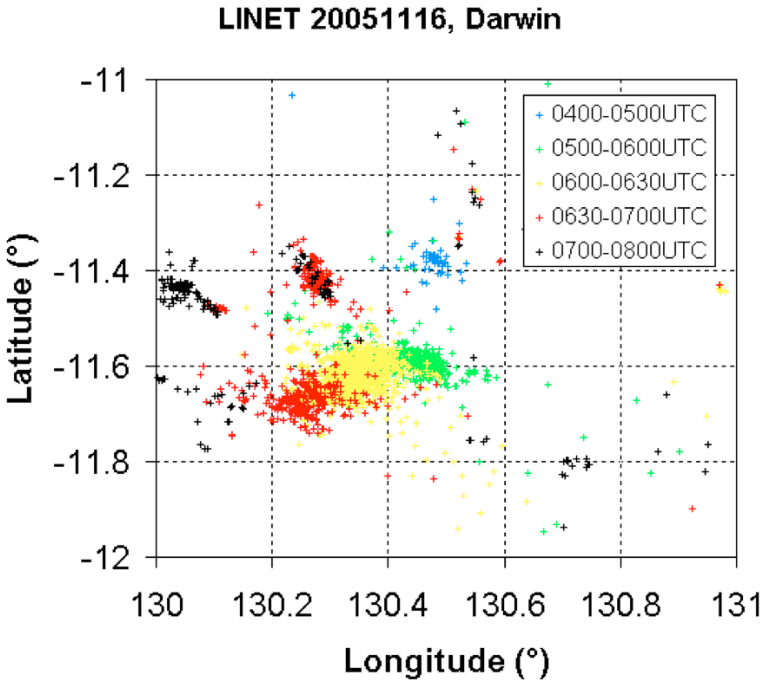

Fig. 6. Lightning flashes (CG and IC) observed by LINET on 16 November 2005 for the Hector thunderstorm that tracked across the Tiwi Islands between roughly 14:30–18:30 LT (05:00–09:00 UTC).

ACPD
12, 16701–16761, 2012

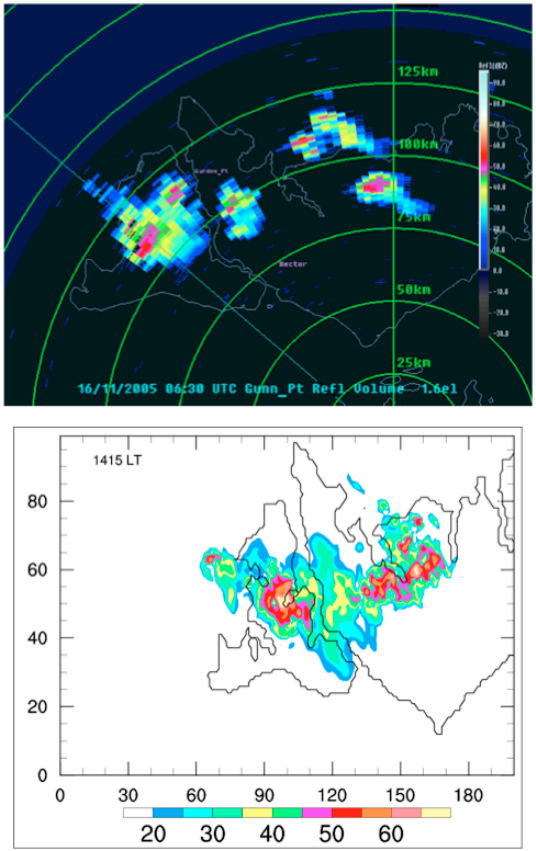

Fig. 7. Comparison of observed radar reflectivity at 16:00 LT (top) to modeled 2.5 km reflectivity at 14:15 LT (bottom). Note the radar echo intensity (dBZ) in the observed radar reflectivity (top) is contoured at every 10 dBZ with the red/magenta interface approximating 50 dBZ. The X and Y axes in the bottom figure show distance in km.

ACPD
12, 16701–16761, 2012

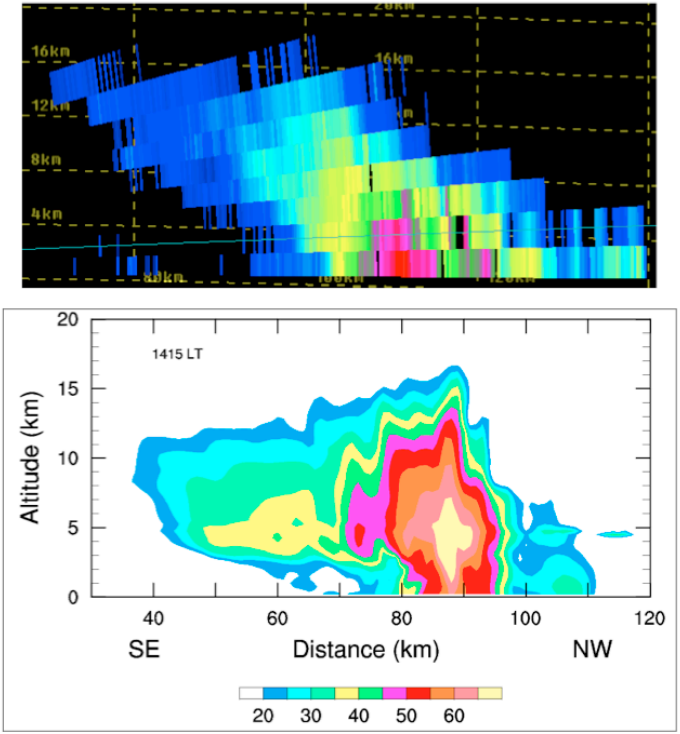

Fig. 8. Vertical cross section comparison of observed radar reflectivity at 16:00 LT (top) to modeled reflectivity at 14:15 LT (bottom). The radar echo density (dBZ) is contoured in both vertical cross sections. Note that the observed radar reflectivity follows the same dBZ scaling as Fig. 7 (top).

ACPD
12, 16701–16761, 2012

Cloud-resolving chemistry simulation of a Hector thunderstorm

K. A. Cummings et al.

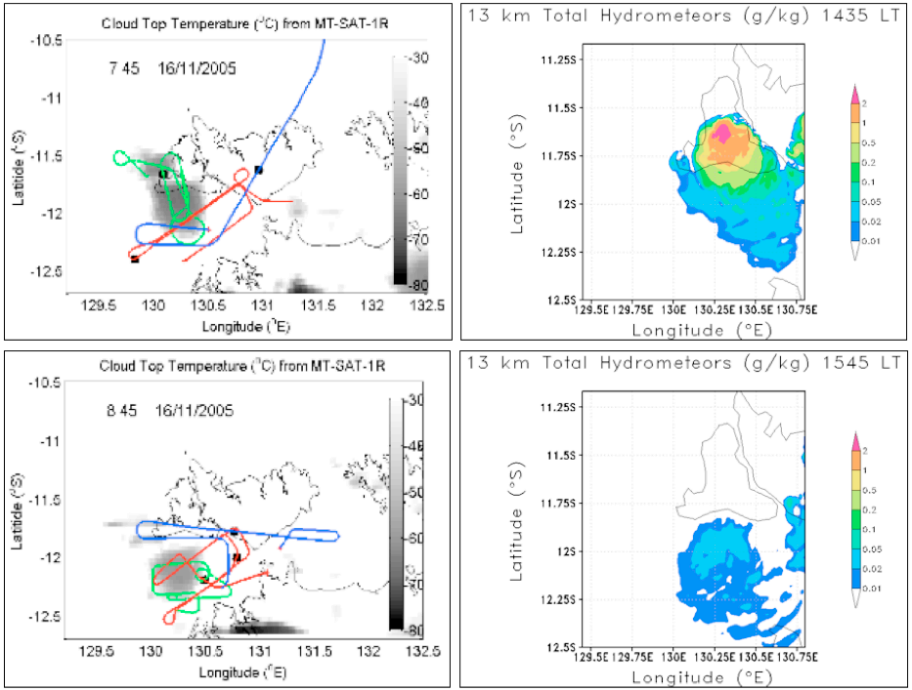

Fig. 9. Comparison of IR satellite anvil observations and aircraft flight tracks (left) with modeled total hydrometeors at 13 km (right). Egrett flight track is in red, Geophysica in green, and Falcon in blue.

ACPD
12, 16701–16761, 2012

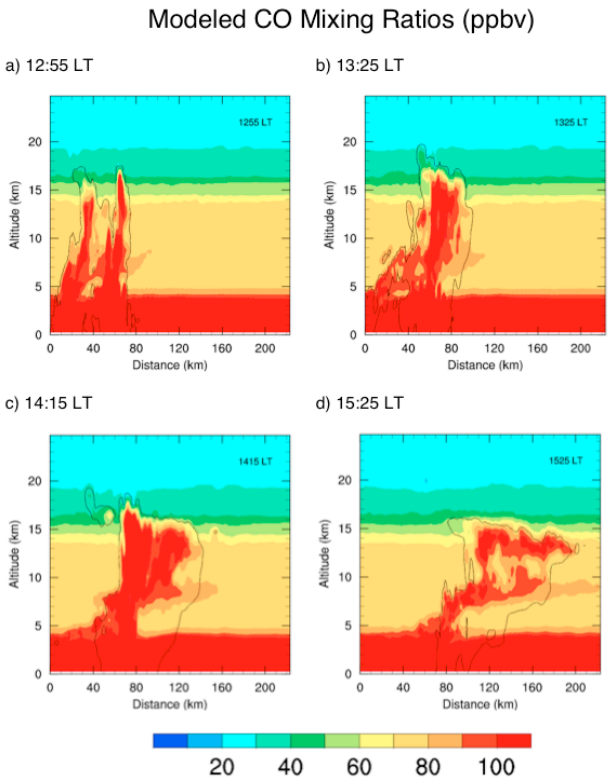

Fig. 10. Time series of vertical cross sections of CO mixing ratios from times **(a)** 12:55 LT, **(b)** 13:25 LT, **(c)** 14:15 LT, **(d)** 15:25 LT, oriented 130° from north. The thin black line indicates the 0.01 g kg^{-1} total condensate contour.

ACPD
12, 16701–16761, 2012

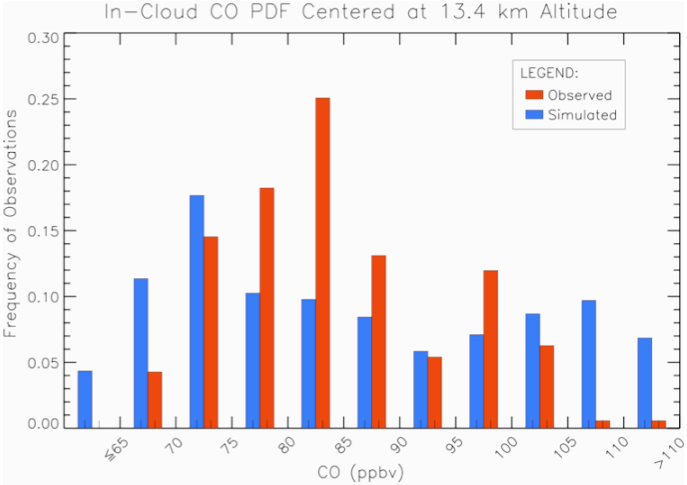

Fig. 11. PDF of observed Egrett (red) and simulated (blue) CO mixing ratios in the model layers centered at 13.4 km given 500 moles NO per flash.

ACPD
12, 16701–16761, 2012

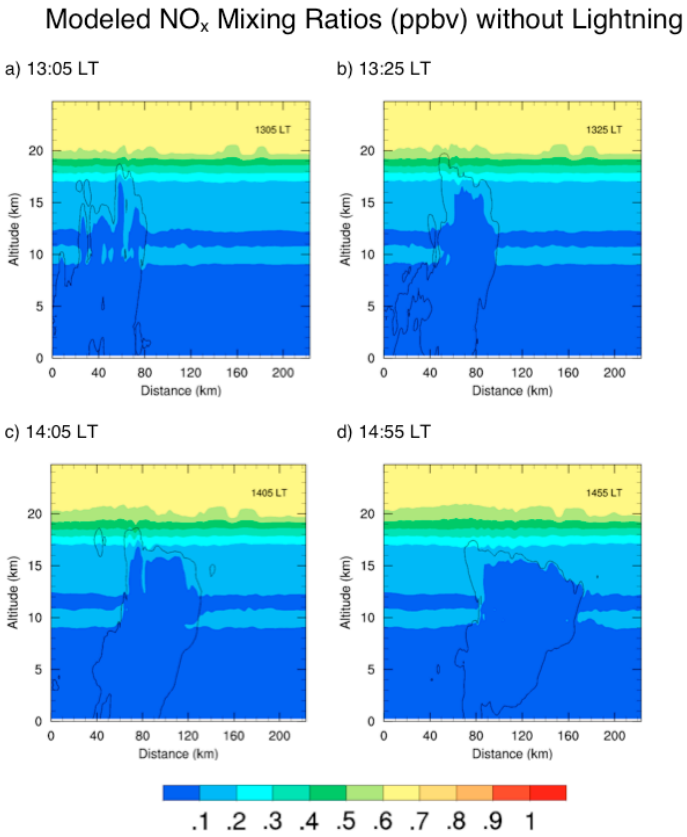

Fig. 12. Time series of vertical cross sections of NO_x mixing ratios for simulations without lightning NO production at **(a)** 13:05 LT, **(b)** 13:25 LT, **(c)** 14:05 LT, and **(d)** 14:55 LT, oriented 130° from north. The thin black line indicates the 0.01 g kg^{-1} total condensate contour.

ACPD
12, 16701–16761, 2012

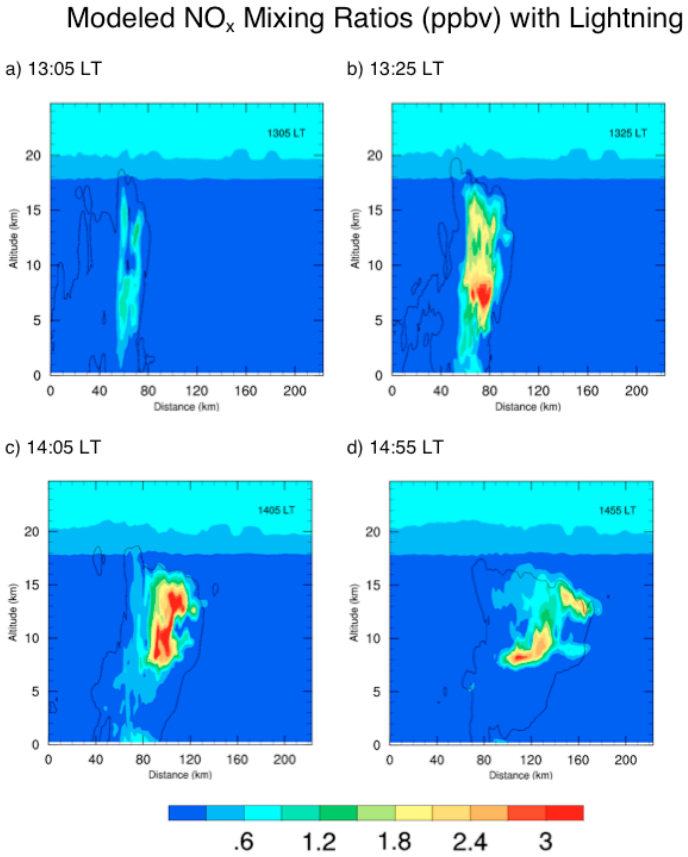

Fig. 13. Time series of vertical cross sections of NO_x mixing ratios for simulations with lightning NO production of 500 moles flash^{-1} at **(a)** 13:05 LT, **(b)** 13:25 LT, **(c)** 14:05 LT, and **(d)** 14:55 LT, oriented 130° from north. The thin black line indicates the 0.01 g kg^{-1} total condensate contour.

ACPD
12, 16701–16761, 2012

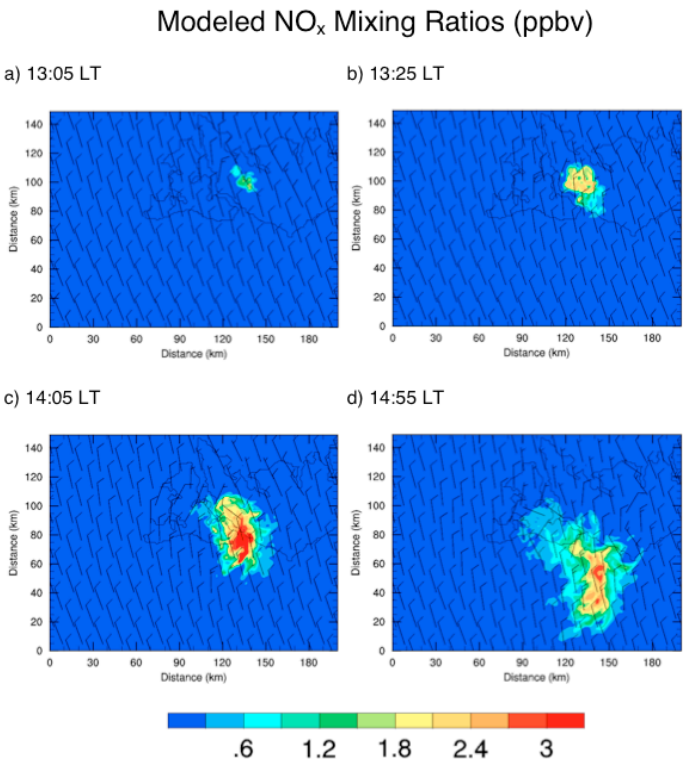

Fig. 14. Time series of NO_x mixing ratios at 13 km for simulations with lightning NO production of 500 moles flash^{-1} at **(a)** 13:05 LT, **(b)** 13:25 LT, **(c)** 14:05 LT, and **(d)** 14:55 LT. Arrows indicate wind vectors at 13 km. Wind speed is reported in m s^{-1}, where a full barb is equivalent to 10 m s^{-1}.

ACPD
12, 16701–16761, 2012

Cloud-resolving chemistry simulation of a Hector thunderstorm

K. A. Cummings et al.

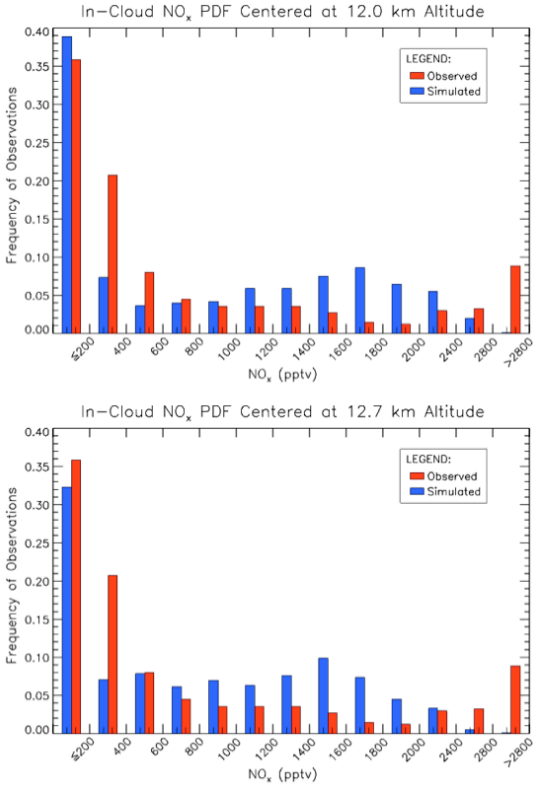

Fig. 15. PDF of NO_x mixing ratios estimated from Egrett observations (red) and simulated (blue) in the model layer centered at 12.0 km and 12.7 km given 500 moles NO per flash.

ACPD
12, 16701–16761, 2012

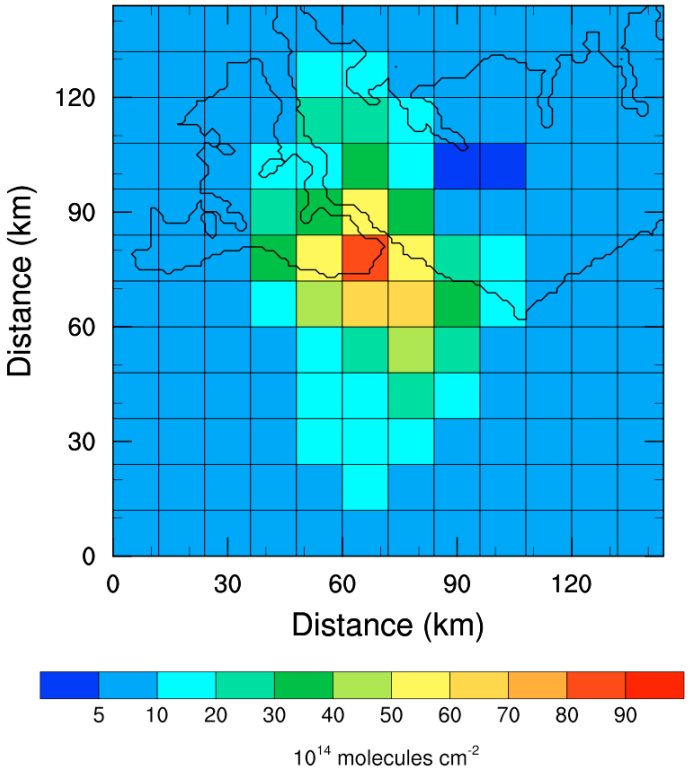

Fig. 16. Partial NO_2 columns from the tropopause (105 mb) to 400 mb for the simulated Hector thunderstorm at 14:45 LT. Each column covers $12 \times 12\,km^2$ area.

ACPD
12, 16701–16761, 2012

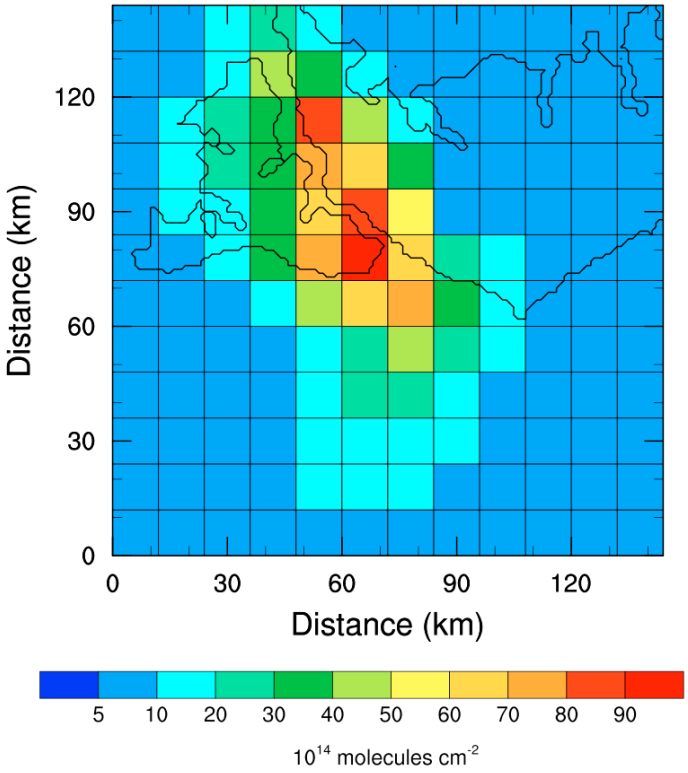

Fig. 17. Partial NO_2 columns from the tropopause (105 mb) to 600 mb for the simulated Hector thunderstorm at 14:45 LT. Each column covers $12 \times 12\,km^2$ area.

ACPD
12, 16701–16761, 2012

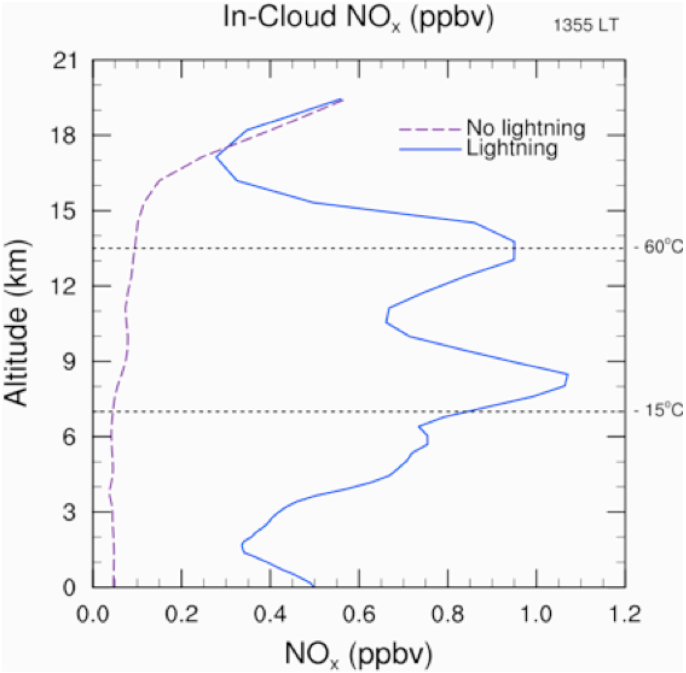

Fig. 18. Average in-cloud NO_x at 13:55 LT for model simulations with and without lightning. Above 17.1 km, values represent the average NO_x directly above the cloud at 17.1 km for model simulations with and without lightning. The dashed lines at 7.0 and 13.5 km represent the usual altitude of the isotherms used for the lower and upper modes, respectively, of the vertical distribution of the lightning NO_x source.

ACPD
12, 16701–16761, 2012

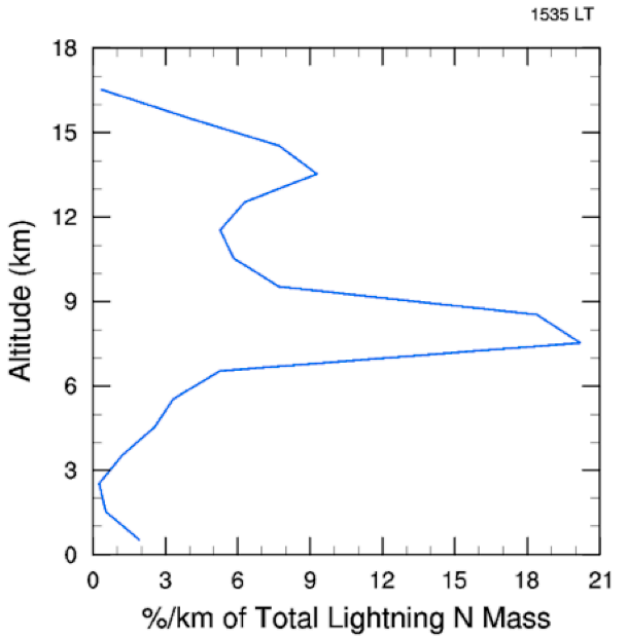

Fig. 19. Vertical distribution of percentage of lightning NO_x mass per kilometer following convection at 15:35 LT given 500 moles NO per flash.

ACPD
12, 16701–16761, 2012

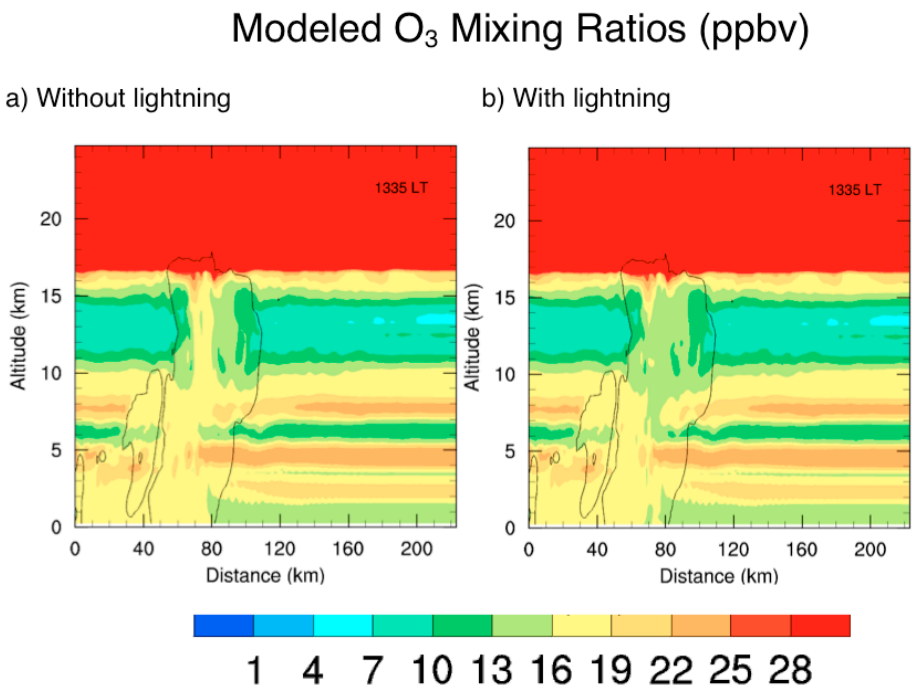

Fig. 20. Vertical cross sections of O_3 mixing ratios, oriented 130° from north, for simulations a) without and b) with lightning NO production. The cross sections occur during a peak in average NO_x production within the layers centered at 12.0 km and 12.7 km. The thin black line indicates the 0.01 g kg^{-1} total condensate contour.

ACPD
12, 16701–16761, 2012

Cloud-resolving chemistry simulation of a Hector thunderstorm

K. A. Cummings et al.